Supporting Information

Effects of Noncanonical Base Pairing on RNA Folding: Structural Context and Spatial Arrangements of G·A Pairs

Wilma K. Olson,[1] Shuxiang Li,[1] Thomas Kaukonen,[1] Andrew V. Colasanti,[1] Yurong Xin,[1] and Xiang-Jun Lu[2]

[1] *Department of Chemistry & Chemical Biology and Center for Quantitative Biology, Rutgers, the State University of New Jersey, Piscataway, New Jersey 08854, USA*

[2] *Department of Biological Sciences, Columbia University, New York, New York 1002, USA*

OVERVIEW

The supporting information includes three tables respectively listing the high-resolution structures that contain the G·A base pairs described in this article (Table S1), the identities and relevant structural features of the selected pairs (Table S2), and the precise identities of depicted G·A-linked structures (Table S3); ten figures respectively illustrating the rigid-body parameters and reference frames used to characterize the spatial arrangements of base pairs (Figure S1), the secondary structures of selected G·A pairs (Figure S2), the observed non-planarity of G·A base associations (Figure S3), the hydrogen bonds linking different modes of G·A pairing (Figure S4), the hydrogen-bonding features of G·A pairs in different spatial forms (Figure S5), the secondary structural contexts of the G·A pairs (Figure S6), the unusual structural settings of an m–M sheared G·A pairs (Figure S7), the secondary structures of selected G·A-mediated multiplets (Figure S8), the relative deformabilities of the major G·A pairing schemes (Figure S9), and the influence of base-pairing on secondary structural pathways (Figure S10).

Table S1. RNA structures containing the noncanonical G·A base pairs examined herein.

PDB_ID[†]	Description[‡]	Ref
	Ribosomes	
3JCS	2.8 ANGSTROM CRYO-EM STRUCTURE OF THE LARGE RIBOSOMAL SUBUNIT FROM THE EUKARYOTIC PARASITE LEISHMANIA	[1]
4V88	THE STRUCTURE OF THE EUKARYOTIC RIBOSOME AT 3.0 A RESOLUTION.	[2]
4V8B	CRYSTAL STRUCTURE ANALYSIS OF RIBOSOMAL DECODING (NEAR-COGNATE TRNA-LEU COMPLEX).	[3]
4V8D	STRUCTURE ANALYSIS OF RIBOSOMAL DECODING (COGNATE TRNA-TYR COMPLEX).	[4]
4V90	THERMUS THERMOPHILUS RIBOSOME	[5]
4V9F	THE RE-REFINED CRYSTAL STRUCTURE OF THE HALOARCULA MARISMORTUI LARGE RIBOSOMAL SUBUNIT AT 2.4 ANGSTROM RESOLUTION: MORE COMPLETE STRUCTURE OF THE L7/L12 AND L1 STALK, L5 AND LX PROTEINS	[6]
4Y4O	CRYSTAL STRUCTURE OF THE THERMUS THERMOPHILUS 70S RIBOSOME WITH RRNA MODIFICATIONS AND BOUND TO PROTEIN Y (YFIA) AT 2.3A RESOLUTION	[7]
5DM6	CRYSTAL STRUCTURE OF THE 50S RIBOSOMAL SUBUNIT FROM DEINOCOCCUS RADIODURANS	[8]
5E81	STRUCTURE OF T. THERMOPHILUS 70S RIBOSOME COMPLEX WITH MRNA AND TRNALYS IN THE A-SITE WITH WOBBLE PAIR	[9]
5IBB	STRUCTURE OF T. THERMOPHILUS 70S RIBOSOME COMPLEX WITH MRNA, TRNAFMET AND COGNATE TRNAVAL IN THE A-SITE	[10]
5NGM	2.9S STRUCTURE OF THE 70S RIBOSOME COMPOSING THE S. AUREUS 100S COMPLEX	[11]
5T2A	CRYOEM STRUCTURE OF THE LEISHMANIA DONOVANI 80S RIBOSOME AT 2.9 ANGSTROM RESOLUTION	[12]
5T5H	STRUCTURE AND ASSEMBLY MODEL FOR THE TRYPANOSOMA CRUZI 60S RIBOSOMAL SUBUNIT	[13]
6ERI	STRUCTURE OF THE CHLOROPLAST RIBOSOME WITH CHL-RRF AND HIBERNATION-PROMOTING FACTOR	[14]
6GSJ	STRUCTURE OF T. THERMOPHILUS 70S RIBOSOME COMPLEX WITH MRNA, TRNAFMET AND COGNATE TRNATHR IN THE A-SITE	[15]
	Ribosomes + antibiotics	
3U4M	CRYSTAL STRUCTURE OF RIBOSOMAL PROTEIN TTHL1 IN COMPLEX WITH 80NT 23S RNA FROM THERMUS THERMOPHILUS	[16]
5FDV	CRYSTAL STRUCTURE OF THE PYRRHOCORICIN ANTIMICROBIAL PEPTIDE BOUND TO THE THERMUS THERMOPHILUS 70S RIBOSOME	[17]
5IB7	STRUCTURE OF T. THERMOPHILUS 70S RIBOSOME COMPLEX WITH MRNA, TRNAFMET, NEAR-COGNATE TRNALYS WITH U-G MISMATCH IN THE A-SITE AND ANTIBIOTIC PAROMOMYCIN	[18]
5J7L	STRUCTURE OF THE 70S E COLI RIBOSOME WITH THE U1052G MUTATION IN THE 16S RRNA BOUND TO TETRACYCLINE	[19]
5TBW	CRYSTAL STRUCTURE OF CHLOROLISSOCLIMIDE BOUND TO THE YEAST 80S RIBOSOME	[20]
6AZ1	CRYO-EM STRUCTURE OF THE SMALL SUBUNIT OF LEISHMANIA RIBOSOME BOUND TO PAROMOMYCIN	[21]
6AZ3	CRYO-EM STRUCTURE OF OF THE LARGE SUBUNIT OF LEISHMANIA RIBOSOME BOUND TO PAROMOMYCIN	[22]
6CFJ	CRYSTAL STRUCTURE OF THE THERMUS THERMOPHILUS 70S RIBOSOME IN COMPLEX WITH HISTIDYL-CAM AND BOUND TO MRNA AND A-, P-, AND E-SITE TRNAS AT 2.8A RESOLUTION	[23]
6EK0	HIGH-RESOLUTION CRYO-EM STRUCTURE OF THE HUMAN 80S RIBOSOME	[24]
	Ribosomal components	
1DFU	CRYSTAL STRUCTURE OF E.COLI RIBOSOMAL PROTEIN L25 COMPLEXED WITH A 5S RRNA FRAGMENT AT 1.8 A RESOLUTION	[25]
1FEU	CRYSTAL STRUCTURE OF RIBOSOMAL PROTEIN TL5, ONE OF THE CTC FAMILY PROTEINS, COMPLEXED WITH A FRAGMENT OF 5S RRNA.	[26]
1G1X	STRUCTURE OF RIBOSOMAL PROTEINS S15, S6, S18, AND 16S RIBOSOMAL RNA	[27]

PDB_ID[†]	Description[‡]	Ref
1HC8	CRYSTAL STRUCTURE OF A CONSERVED RIBOSOMAL PROTEIN-RNA COMPLEX	[28]
1KUQ	CRYSTAL STRUCTURE OF T3C MUTANT S15 RIBOSOMAL PROTEIN IN COMPLEX WITH 16S RRNA	[29]
1MMS	CRYSTAL STRUCTURE OF THE RIBOSOMAL PROTEIN L11-RNA COMPLEX	[30]
1MZP	STRUCTURE OF THE L1 PROTUBERANCE IN THE RIBOSOME	[31]
2A43	CRYSTAL STRUCTURE OF A LUTEOVIRAL RNA PSEUDOKNOT AND MODEL FOR A MINIMAL RIBOSOMAL FRAMESHIFTING MOTIF	[32]
2BH2	CRYSTAL STRUCTURE OF E. COLI 5-METHYLURIDINE METHYLTRANSFERASE RUMA IN COMPLEX WITH RIBOSOMAL RNA SUBSTRATE AND S-ADENOSYLHOMOCYSTEINE.	[33]
	Riboswitches	
1Y26	A-RIBOSWITCH-ADENINE COMPLEX	[34]
1Y27	G-RIBOSWITCH-GUANINE COMPLEX	[35]
2GDI	CRYSTAL STRUCTURE OF THIAMINE PYROPHOSPHATE-SPECIFIC RIBOSWITCH IN COMPLEX WITH THIAMINE PYROPHOSPHATE	[36]
2QWY	SAM-II RIBOSWITCH BOUND TO S-ADENOSYLMETHIONINE	[37]
2YGH	SAM-I RIBOSWITCH WITH A G2NA MUTATION IN THE KINK TURN IN COMPLEX WITH S-ADENOSYLMETHIONINE	[38]
3D0U	CRYSTAL STRUCTURE OF LYSINE RIBOSWITCH BOUND TO LYSINE	[39]
3D2V	STRUCTURE OF THE EUKARYOTIC TPP-SPECIFIC RIBOSWITCH BOUND TO THE ANTIBACTERIAL COMPOUND PYRITHIAMINE PYROPHOSPHATE	[40]
3DIL	CRYSTAL STRUCTURE OF THE THERMOTOGA MARITIMA LYSINE RIBOSWITCH BOUND TO LYSINE	[41]
3E5C	CRYSTAL STRUCTURE OF THE SMK BOX (SAM-III) RIBOSWITCH WITH SAM	[42]
3EGZ	CRYSTAL STRUCTURE OF AN IN VITRO EVOLVED TETRACYCLINE APTAMER AND ARTIFICIAL RIBOSWITCH	[43]
3F2Q	CRYSTAL STRUCTURE OF THE FMN RIBOSWITCH BOUND TO FMN	[44]
3IVN	STRUCTURE OF THE U65C MUTANT A-RIBOSWITCH APTAMER FROM THE BACILLUS SUBTILIS PBUE OPERON	[45]
3K1V	COCRYSTAL STRUCTURE OF A MUTANT CLASS-I PREQ1 RIBOSWITCH	[46]
3LA5	X-RAY CRYSTAL STRUCTURE OF MC6 RNA RIBOSWITCH BOUND TO AZACYTOSINE	[47]
3MXH	NATIVE STRUCTURE OF A C-DI-GMP RIBOSWITCH FROM V. CHOLERAE	[48]
3NPQ	STRUCTURE OF THE S-ADENOSYLHOMOCYSTEINE RIBOSWITCH AT 2.18 A	[49]
3OXE	CRYSTAL STRUCTURE OF GLYCINE RIBOSWITCH, MN2+ SOAKED	[50]
3PDR	CRYSTAL STRUCTURE OF MANGANESE BOUND M-BOX RNA	[51]
3Q3Z	STRUCTURE OF A C-DI-GMP-II RIBOSWITCH FROM C. ACETOBUTYLICUM BOUND TO C-DI-GMP	[52]
3Q50	STRUCTURAL ANALYSIS OF A CLASS I PREQ1 RIBOSWITCH APTAMER IN THE METABOLITE-BOUND STATE	[53]
3RKF	CRYSTAL STRUCTURE OF GUANINE RIBOSWITCH C61U/G37A DOUBLE MUTANT BOUND TO THIO-GUANINE	[54]
3SKI	CRYSTAL STRUCTURE OF THE 2'- DEOXYGUANOSINE RIBOSWITCH BOUND TO 2'-DEOXYGUANOSINE	[55]
3SKL	CRYSTAL STRUCTURE OF THE 2'- DEOXYGUANOSINE RIBOSWITCH BOUND TO 2'-DEOXYGUANOSINE, IRIDIUM HEXAMMINE SOAK	[56]
3SUX	CRYSTAL STRUCTURE OF THF RIBOSWITCH, BOUND WITH THF	[57]
3V7E	CRYSTAL STRUCTURE OF YBXF BOUND TO THE SAM-I RIBOSWITCH APTAMER	[58]
4AOB	SAM-I RIBOSWITCH CONTAINING THE T. SOLENOPSAE KT-23 IN COMPLEX WITH S-ADENOSYL METHIONINE	[59]
4ENC	CRYSTAL STRUCTURE OF FLUORIDE RIBOSWITCH	[60]
4FEN	CRYSTAL STRUCTURE OF THE A24U/U25A/A46G MUTANT XPT-PBUX GUANINE RIBOSWITCH APTAMER DOMAIN IN COMPLEX WITH HYPOXANTHINE	[61]
4FRG	CRYSTAL STRUCTURE OF THE COBALAMIN RIBOSWITCH APTAMER DOMAIN	[62]
4JF2	STRUCTURE OF A CLASS II PREQ1 RIBOSWITCH REVEALS LIGAND RECOGNITION BY A NEW FOLD	[63]
4L81	STRUCTURE OF THE SAM-I/IV RIBOSWITCH (ENV87(DELTAU92, DELTAG93))	[64]
4LVW	STRUCTURE OF THE THF RIBOSWITCH BOUND TO 7-DEAZAGUANINE	[65]
4LX6	X-RAY CRYSTAL STRUCTURE OF THE M6C' RIBOSWITCH APTAMER BOUND TO 2-AMINOPYRIMIDO[4,5-D]PYRIMIDIN-4(3H)-ONE (PPAO)	[66]
4QLM	YDAO RIBOSWITCH BINDING TO C-DI-AMP	[67]

PDB_ID[†]	Description[‡]	Ref
4RUM	CRYSTAL STRUCTURE OF THE NICO TRANSITION-METAL RIBOSWITCH BOUND TO COBALT	[68]
4RZD	CRYSTAL STRUCTURE OF A PREQ1 RIBOSWITCH	[69]
4XNR	VIBRIO VULNIFICUS ADENINE RIBOSWITCH APTAMER DOMAIN, SYNTHESIZED BY POSITION-SELECTIVE LABELING OF RNA (PLOR), IN COMPLEX WITH ADENINE	[70]
4XWF	CRYSTAL STRUCTURE OF THE ZMP RIBOSWITCH AT 1.80 ANGSTROM	[71]
4Y1J	LACTOCOCCUS LACTIS YYBP-YKOY MN RIBOSWITCH A41U BINDING SITE MUTANT IN PRESENCE OF MN2+	[72]
4Y1M	AN ESCHERICHIA COLI YYBP-YKOY MN RIBOSWITCH IN THE MN2+-FREE STATE	[73]
4YAZ	3',3'-CGAMP RIBOSWITCH BOUND WITH 3',3'-CGAMP	[74]
4ZNP	THE STRUCTURE OF A PFI RIBOSWITCH BOUND TO ZMP	[75]
5C45	SELECTIVE SMALL MOLECULE INHIBITION OF THE FMN RIBOSWITCH	[76]
5D5L	PREQ1-II RIBOSWITCH WITH AN ENGINEERED G-U WOBBLE PAIR BOUND TO CS+	[*]
5DDP	L-GLUTAMINE RIBOSWITCH BOUND WITH L-GLUTAMINE	[77]
5FJC	SAM-I RIBOSWITCH BEARING THE H. MARISMORTUI KT-7 VARIANT C-2BU	[78]
5NWQ	THE STRUCTURE OF THE THERMOBIFIDA FUSCA GUANIDINE III RIBOSWITCH WITH GUANIDINE.	[79]
5SWD	STRUCTURE OF THE ADENINE RIBOSWITCH APTAMER DOMAIN IN AN INTERMEDIATE-BOUND STATE	[80]
5T83	STRUCTURE OF A GUANIDINE-I RIBOSWITCH FROM S. ACIDOPHILUS	[81]
5U3G	STRUCTURE OF THE DICKEYA DADANTII YKKC RIBOSWITCH BOUND TO GUANIDINIUM	[82]
6CB3	CRYSTAL STRUCTURE OF THE L.LACTIS YKOY RIBOSWITCH BOUND TO CADMIUM	[83]
6CK5	PRPP RIBOSWITCH FROM T. MATHRANII BOUND TO PRPP	[84]
6DN2	CRYSTAL STRUCTURE OF THE FMN RIBOSWITCH BOUND TO BRX1354 SPLIT RNA	[85]
6FZ0	CRYSTAL STRUCTURE OF THE METY SAM V RIBOSWITCH	[86]
	Ribozymes	
1HMH	THREE-DIMENSIONAL STRUCTURE OF A HAMMERHEAD RIBOZYME	[87]
1KXK	CRYSTAL STRUCTURE OF A RNA MOLECULE CONTAINING DOMAIN 5 AND 6 OF THE YEAST AI5G GROUP II SELF-SPLICING INTRON	[88]
1U9S	CRYSTAL STRUCTURE OF THE SPECIFICITY DOMAIN OF RIBONUCLEASE P OF THE A-TYPE	[89]
1YLS	CRYSTAL STRUCTURE OF SELENIUM-MODIFIED DIELS-ALDER RIBOZYME COMPLEXED WITH THE PRODUCT OF THE REACTION BETWEEN N-PENTYLMALEIMIDE AND COVALENTLY ATTACHED 9-HYDROXYMETHYLANTHRACENE	[90]
2OEU	FULL-LENGTH HAMMERHEAD RIBOZYME WITH MN(II) BOUND	[91]
2OIU	L1 RIBOZYME LIGASE CIRCULAR ADDUCT	[92]
2P7E	VANADATE AT THE ACTIVE SITE OF A SMALL RIBOZYME SUGGESTS A ROLE FOR WATER IN TRANSITION-STATE STABILIZATION	[93]
2QUS	HAMMERHEAD RIBOZYME G12A MUTANT PRE-CLEAVAGE	[94]
2QUW	HAMMERHEAD RIBOZYME G12A MUTANT AFTER CLEAVAGE	[95]
2R8S	HIGH RESOLUTION STRUCTURE OF A SPECIFIC SYNTHETIC FAB BOUND TO P4-P6 RNA RIBOZYME DOMAIN	[96]
2Z75	T. TENGCONGENSIS GLMS RIBOZYME BOUND TO GLUCOSAMINE-6-PHOSPHATE	[97]
359D	INHIBITION OF THE HAMMERHEAD RIBOZYME CLEAVAGE REACTION BY SITE-SPECIFIC BINDING OF TB(III)	[98]
3BBM	MINIMALLY JUNCTIONED HAIRPIN RIBOZYME INCORPORATES A38C AND 2'O-ME MODIFICATION AT ACTIVE SITE	[99]
3CUL	AMINOACYL-TRNA SYNTHETASE RIBOZYME	[100]
3G9C	CRYSTAL STRUCTURE OF THE PRODUCT BACILLUS ANTHRACIS GLMS RIBOZYME	[101]
3GS5	AN ALL-RNA HAIRPIN RIBOZYME A38N1DA VARIANT WITH A PRODUCT MIMIC SUBSTRATE STRAND	[102]
3HHN	CRYSTAL STRUCTURE OF CLASS I LIGASE RIBOZYME SELF-LIGATION PRODUCT, IN COMPLEX WITH U1A RBD	[103]
3NKB	A 1.9A CRYSTAL STRUCTURE OF THE HDV RIBOZYME PRECLEAVAGE SUGGESTS BOTH LEWIS ACID AND GENERAL ACID MECHANISMS CONTRIBUTE TO PHOSPHODIESTER CLEAVAGE	[104]
4FAR	STRUCTURE OF OCEANOBACILLUS IHEYENSIS GROUP II INTRON IN THE PRESENCE OF K+, MG2+ AND 5'-EXON	[105]
4OJI	CRYSTAL STRUCTURE OF TWISTER RIBOZYME	[106]

PDB_ID[†]	Description[‡]	Ref
4P95	SPECIATION OF A GROUP I INTRON INTO A LARIAT CAPPING RIBOZYME (CIRCULARLY PERMUTATED RIBOZYME)	[107]
4PR6	A SECOND LOOK AT THE HDV RIBOZYME STRUCTURE AND DYNAMICS.	[108]
4PRF	A SECOND LOOK AT THE HDV RIBOZYME STRUCTURE AND DYNAMICS.	[109]
4RGE	CRYSTAL STRUCTURE OF THE IN-LINE ALIGNED ENV22 TWISTER RIBOZYME	[110]
5DH6	TWO DIVALENT METAL IONS AND CONFORMATIONAL CHANGES PLAY ROLES IN THE HAMMERHEAD RIBOZYME CLEAVAGE REACTION-G12A MUTANT IN MG2+	[111]
5K7D	THE STRUCTURE OF NATIVE PISTOL RIBOZYME, BOUND TO IRIDIUM	[112]
5KTJ	CRYSTAL STRUCTURE OF PISTOL, A CLASS OF SELF-CLEAVING RIBOZYME	[113]
5T5A	CRYSTAL STRUCTURE OF THE TWISTER SISTER (TS) RIBOZYME AT 2.0 ANGSTROM	[114]
5UZ6	RNA HAIRPIN STRUCTURE CONTAINING 2-MEIMP-OLIGO ANALOGUE	[115]
	Ribozyme fragment	
3FS0	CLASS II LIGASE RIBOZYME PRODUCT-TEMPLATE DUPLEX, STRUCTURE 2	[116]
3FTM	CLASS II LIGASE RIBOZYME PRODUCT-TEMPLATE DUPLEX, STRUCTURE 1	[117]
	tRNA	
1C0A	CRYSTAL STRUCTURE OF THE E. COLI ASPARTYL-TRNA SYNTHETASE : TRNAASP : ASPARTYL-ADENYLATE COMPLEX	[118]
1EVV	CRYSTAL STRUCTURE OF YEAST PHENYLALANINE TRANSFER RNA AT 2.0 A RESOLUTION	[119]
1GAX	CRYSTAL STRUCTURE OF THERMUS THERMOPHILUS VALYL-TRNA SYNTHETASE COMPLEXED WITH TRNA(VAL) AND VALYL-ADENYLATE ANALOGUE	[120]
1H3E	TYROSYL-TRNA SYNTHETASE FROM THERMUS THERMOPHILUS COMPLEXED WITH WILD-TYPE TRNATYR(GUA) AND WITH ATP AND TYROSINOL	[121]
1H4S	PROLYL-TRNA SYNTHETASE FROM THERMUS THERMOPHILUS COMPLEXED WITH TRNAPRO(CGG) AND A PROLYL-ADENYLATE ANALOGUE	[122]
1IL2	CRYSTAL STRUCTURE OF THE E. COLI ASPARTYL-TRNA SYNTHETASE:YEAST TRNAASP:ASPARTYL-ADENYLATE COMPLEX	[123]
1J1U	CRYSTAL STRUCTURE OF ARCHAEAL TYROSYL-TRNA SYNTHETASE COMPLEXED WITH TRNA(TYR) AND L-TYROSINE	[124]
1N78	CRYSTAL STRUCTURE OF THERMUS THERMOPHILUS GLUTAMYL-TRNA SYNTHETASE COMPLEXED WITH TRNA(GLU) AND GLUTAMOL-AMP.	[125]
1QF6	STRUCTURE OF E. COLI THREONYL-TRNA SYNTHETASE COMPLEXED WITH ITS COGNATE TRNA	[126]
1QU2	INSIGHTS INTO EDITING FROM AN ILE-TRNA SYNTHETASE STRUCTURE WITH TRNA(ILE) AND MUPIROCIN	[127]
1SER	THE 2.9 ANGSTROMS CRYSTAL STRUCTURE OF T. THERMOPHILUS SERYL-TRNA SYNTHETASE COMPLEXED WITH TRNA SER	[128]
1YFG	YEAST INITIATOR TRNA	[129]
2AZX	CHARGED AND UNCHARGED TRNAS ADOPT DISTINCT CONFORMATIONS WHEN COMPLEXED WITH HUMAN TRYPTOPHANYL-TRNA SYNTHETASE	[130]
2BTE	THERMUS THERMOPHILUS LEUCYL-TRNA SYNTHETASE COMPLEXED WITH A TRNALEU TRANSCRIPT IN THE POST-EDITING CONFORMATION AND A POST-TRANSFER EDITING SUBSTRATE ANALOGUE	[131]
2CSX	CRYSTAL STRUCTURE OF AQUIFEX AEOLICUS METHIONYL-TRNA SYNTHETASE COMPLEXED WITH TRNA(MET)	[132]
2DLC	CRYSTAL STRUCTURE OF THE TERNARY COMPLEX OF YEAST TYROSYL-TRNA SYNTHETASE	[133]
2DU3	CRYSTAL STRUCTURE OF ARCHAEOGLOBUS FULGIDUS O-PHOSPHOSERYL-TRNA SYNTHETASE COMPLEXED WITH TRNACYS AND O-PHOSPHOSERINE	[134]
2ZUE	CRYSTAL STRUCTURE OF PYROCOCCUS HORIKOSHII ARGINYL-TRNA SYNTHETASE COMPLEXED WITH TRNA(ARG) AND AN ATP ANALOG (ANP)	[135]
2ZY6	CRYSTAL STRUCTURE OF A TRUNCATED TRNA, TPHE39A	[136]
3AKZ	CRYSTAL STRUCTURE OF THERMOTOGA MARITIMA NONDISCRIMINATING GLUTAMYL-TRNA SYNTHETASE IN COMPLEX WITH TRNAGLN AND A GLUTAMYL-AMP ANALOG	[137]
3AM1	CRYSTAL STRUCTURE OF O-PHOSPHOSERYL-TRNA KINASE COMPLEXED WITH ANTICODON-STEM/LOOP TRUNCATED TRNA(SEC)	[138]
3RG5	CRYSTAL STRUCTURE OF MOUSE TRNA(SEC)	[139]

PDB_ID[†]	Description[‡]	Ref
3ZGZ	TERNARY COMPLEX OF E. COLI LEUCYL-TRNA SYNTHETASE, TRNA(LEU) AND TOXIC MOIETY FROM AGROCIN 84 (TM84) IN AMINOACYLATION-LIKE CONFORMATION	[140]
4JRC	DISTAL STEM I REGION FROM G. KAUSTOPHILUS GLYQS T BOX RNA	[141]
4K50	RHINOVIRUS 16 POLYMERASE ELONGATION COMPLEX (R1_FORM)	[142]
4P5J	CRYSTAL STRUCTURE OF THE TRNA-LIKE STRUCTURE FROM TURNIP YELLOW MOSAIC VIRUS (TYMV), A TRNA MIMICKING RNA	[143]
4QEI	TWO DISTINCT CONFORMATIONAL STATES OF GLYRS CAPTURED IN CRYSTAL LATTICE	[144]
4RDX	STRUCTURE OF HISTIDINYL-TRNA SYNTHETASE IN COMPLEX WITH TRNA(HIS)	[145]
5AXM	CRYSTAL STRUCTURE OF THG1 LIKE PROTEIN (TLP) WITH TRNA(PHE)	[146]
5BTP	FUSOBACTERIUM ULCERANS ZTP RIBOSWITCH BOUND TO ZMP	[147]
5CCB	CRYSTAL STRUCTURE OF HUMAN M1A58 METHYLTRANSFERASE IN A COMPLEX WITH TRNA3LYS AND SAH	[148]
5L4O	STRUCTURE OF AN E.COLI INITIATOR TRNAFMET A1-U72 VARIANT	[149]
5ZQ8	CRYSTAL STRUCTURE OF SPRLMCD WITH U747 STEMLOOP RNA	[150]
6CU1	X-RAY STRUCTURE OF THE S. TYPHIMURIUM YRLA EFFECTOR-BINDING MODULE	[151]
6DU4	CRYSTAL STRUCTURE OF HMETTL16 CATALYTIC DOMAIN IN COMPLEX WITH MAT2A 3'UTR HAIRPIN 1	[152]
	Aptamers	
1ET4	CRYSTAL STRUCTURE OF A VITAMIN B12 BINDING RNA APTAMER WITH LIGAND AT 2.3 A	[153]
1F1T	CRYSTAL STRUCTURE OF THE MALACHITE GREEN APTAMER COMPLEXED WITH TETRAMETHYL-ROSAMINE	[154]
1OOA	CRYSTAL STRUCTURE OF NF-KB(P50)2 COMPLEXED TO A HIGH-AFFINITY RNA APTAMER	[155]
2JLT	CRYSTAL STRUCTURE OF AN RNA KISSING COMPLEX	[156]
3EGZ	CRYSTAL STRUCTURE OF AN IN VITRO EVOLVED TETRACYCLINE APTAMER AND ARTIFICIAL RIBOSWITCH	[157]
3Q50	STRUCTURAL ANALYSIS OF A CLASS I PREQ1 RIBOSWITCH APTAMER IN THE METABOLITE-BOUND STATE	[158]
3V7E	CRYSTAL STRUCTURE OF YBXF BOUND TO THE SAM-I RIBOSWITCH APTAMER	[159]
4FEN	CRYSTAL STRUCTURE OF THE A24U/U25A/A46G MUTANT XPT-PBUX GUANINE RIBOSWITCH APTAMER DOMAIN IN COMPLEX WITH HYPOXANTHINE	[160]
4FRG	CRYSTAL STRUCTURE OF THE COBALAMIN RIBOSWITCH APTAMER DOMAIN	[161]
4KZD	CRYSTAL STRUCTURE OF AN RNA APTAMER IN COMPLEX WITH FLUOROPHORE AND FAB	[162]
4L81	STRUCTURE OF THE SAM-I/IV RIBOSWITCH (ENV87(DELTAU92, DELTAG93))	[163]
4M4O	CRYSTAL STRUCTURE OF THE APTAMER MINE-LYSOZYME COMPLEX	[*]
4M6D	CRYSTAL STRUCTURE OF THE APTAMER MINF-LYSOZYME COMPLEX.	[*]
4TS2	CRYSTAL STRUCTURE OF THE SPINACH RNA APTAMER IN COMPLEX WITH DFHBI, MAGNESIUM IONS	[164]
5KPY	STRUCTURE OF A 5-HYDROXYTRYPTOPHAN APTAMER	[165]
5OB3	ISPINACH APTAMER	[166]
6C63	CRYSTAL STRUCTURE OF THE MANGO-II FLUORESCENT APTAMER BOUND TO TO1-BIOTIN	[167]
6C65	CRYSTAL STRUCTURE OF THE MANGO-II-A22U FLUORESCENT APTAMER BOUND TO TO1-BIOTIN	[168]
6CF2	CRYSTAL STRUCTURE OF HIV-1 REV (RESIDUES 1-93)-RNA APTAMER COMPLEX	[169]
	Duplex RNA	
1CSL	CRYSTAL STRUCTURE OF THE RRE HIGH AFFINITY SITE	[170]
1D4R	29-MER FRAGMENT OF HUMAN SRP RNA HELIX 6	[171]
1DUQ	CRYSTAL STRUCTURE OF THE REV BINDING ELEMENT OF HIV-1	[172]
1JBR	CRYSTAL STRUCTURE OF THE RIBOTOXIN RESTRICTOCIN AND A 31-MER SRD RNA INHIBITOR	[173]
1LNT	CRYSTAL STRUCTURE OF THE HIGHLY CONSERVED RNA INTERNAL LOOP OF SRP	[174]
1M5K	CRYSTAL STRUCTURE OF A HAIRPIN RIBOZYME IN THE CATALYTICALLY-ACTIVE CONFORMATION	[175]
1MHK	CRYSTAL STRUCTURE ANALYSIS OF A 26MER RNA MOLECULE, REPRESENTING A NEW RNA MOTIF, THE HOOK-TURN	[176]

PDB_ID[†]	Description[‡]	Ref
1SA9	CRYSTAL STRUCTURE OF THE RNA OCTAMER GGCGAGCC	[177]
1SAQ	CRYSTAL STRUCTURE OF THE RNA OCTAMER GIC(GA)GCC	[178]
2ANN	CRYSTAL STRUCTURE (I) OF NOVA-1 KH1/KH2 DOMAIN TANDEM WITH 25 NT RNA HAIRPIN	[179]
2EZ6	CRYSTAL STRUCTURE OF AQUIFEX AEOLICUS RNASE III (D44N) COMPLEXED WITH PRODUCT OF DOUBLE-STRANDED RNA PROCESSING	[180]
2GJW	RNA RECOGNITION AND CLEAVAGE BY AN SPLICING ENDONUCLEASE	[181]
2H1M	SYNTHESIS, OXIDATION BEHAVIOR, CRYSTALLIZATION AND STRUCTURE OF 2'-METHYLSELENO GUANOSINE CONTAINING RNAS	[182]
2HVY	CRYSTAL STRUCTURE OF AN H/ACA BOX RNP FROM PYROCOCCUS FURIOSUS	[183]
2NUE	CRYSTAL STRUCTURE OF RNASE III FROM AQUIFEX AEOLICUS COMPLEXED WITH DS-RNA AT 2.9-ANGSTROM RESOLUTION	[184]
2O3Y	CRYSTAL STRUCTURE OF THE HOMO SAPIENS CYTOPLASMIC RIBOSOMAL DECODING SITE IN PRESENCE OF PAROMAMINE DERIVATIVE NB30	[185]
2OE5	1.5 A X-RAY CRYSTAL STRUCTURE OF APRAMYCIN COMPLEX WITH RNA FRAGMENT GGCGUCGCUAGUACCG/GGUACUAAAAGUCGCCC CONTAINING THE HUMAN RIBOSOMAL DECODING A SITE: RNA CONSTRUCT WITH 3'-OVERHANG	[186]
2OE8	1.8 A X-RAY CRYSTAL STRUCTURE OF APRAMYCIN COMPLEX WITH RNA FRAGMENT GGGCGUCGCUAGUACC/CGGUACUAAAAGUCGCC CONTAINING THE HUMAN RIBOSOMAL DECODING A SITE: RNA CONSTRUCT WITH 5'-OVERHANG	[187]
2OZB	STRUCTURE OF A HUMAN PRP31-15.5K-U4 SNRNA COMPLEX	[188]
2VPL	THE STRUCTURE OF THE COMPLEX BETWEEN THE FIRST DOMAIN OF L1 PROTEIN FROM THERMUS THERMOPHILUS AND MRNA FROM METHANOCOCCUS JANNASCHII	[189]
354D	STRUCTURE OF LOOP E FROM E. COLI 5S RRNA	[190]
364D	3.0 A STRUCTURE OF FRAGMENT I FROM E. COLI 5S RRNA	[191]
3AGV	CRYSTAL STRUCTURE OF A HUMAN IGG-APTAMER COMPLEX	[192]
3CJZ	EFFECTS OF N2,N2-DIMETHYLGUANOSINE ON RNA STRUCTURE AND STABILITY: CRYSTAL STRUCTURE OF AN RNA DUPLEX WITH TANDEM M22G:A PAIRS	[193]
3FTE	CRYSTAL STRUCTURE OF A. AEOLICUS KSGA IN COMPLEX WITH RNA	[194]
3FTF	CRYSTAL STRUCTURE OF A. AEOLICUS KSGA IN COMPLEX WITH RNA AND SAH	[195]
3HAX	CRYSTAL STRUCTURE OF A SUBSTRATE-BOUND GAR1-MINUS H/ACA RNP FROM PYROCOCCUS FURIOSUS	[196]
3HJW	STRUCTURE OF A FUNCTIONAL RIBONUCLEOPROTEIN PSEUDOURIDINE SYNTHASE BOUND TO A SUBSTRATE RNA	[197]
3IAB	CRYSTAL STRUCTURE OF RNASE P /RNASE MRP PROTEINS POP6, POP7 IN A COMPLEX WITH THE P3 DOMAIN OF RNASE MRP RNA	[198]
3MOJ	STRUCTURE OF THE RNA BINDING DOMAIN OF THE BACILLUS SUBTILIS YXIN PROTEIN COMPLEXED WITH A FRAGMENT OF 23S RIBOSOMAL RNA	[199]
3MQK	CBF5-NOP10-GAR1 COMPLEX BINDING WITH 17MER RNA CONTAINING ACA TRINUCLEOTIDE	[200]
3NMU	CRYSTAL STRUCTURE OF SUBSTRATE-BOUND HALFMER BOX C/D RNP	[201]
3NVI	STRUCTURE OF N-TERMINAL TRUNCATED NOP56/58 BOUND WITH L7AE AND BOX C/D RNA	[202]
3R9X	CRYSTAL STRUCTURE OF ERA IN COMPLEX WITH MGGDPNP, NUCLEOTIDES 1506-1542 OF 16S RIBOSOMAL RNA, AND KSGA	[203]
3RW6	STRUCTURE OF NUCLEAR RNA EXPORT FACTOR TAP BOUND TO CTE RNA	[204]
3TD0	CRYSTAL STRUCTURE OF THE BACTERIAL A1408G-MUTANT AND THE PROTOZOA CYTOPLASMIC RIBOSOMAL DECODING SITE	[205]
3TRZ	MOUSE LIN28A IN COMPLEX WITH LET-7D MICRORNA PRE-ELEMENT	[206]
4AL5	CRYSTAL STRUCTURE OF THE CSY4-CRRNA PRODUCT COMPLEX	[207]
4BW0	THE MOLECULAR RECOGNITION OF KINK TURN STRUCTURE BY THE L7AE CLASS OF PROTEINS	[208]
4C4W	STRUCTURE OF A RARE, NON-STANDARD SEQUENCE K-TURN BOUND BY L7AE PROTEIN	[209]
4C8Y	CAS6 (TTHA0078) SUBSTRATE MIMIC COMPLEX	[210]
4C8Z	CAS6 (TTHA0078) PRODUCT COMPLEX	[211]
4K27	MYOTONIC DYSTROPHY TYPE 2 RNA: STRUCTURAL STUDIES AND DESIGNED SMALL MOLECULES THAT MODULATE RNA FUNCTION	[*]
4K31	CRYSTAL STRUCTURE OF APRAMYCIN BOUND TO THE LEISHMANIAL RRNA A-SITE	[212]
4M4O	CRYSTAL STRUCTURE OF THE APTAMER MINE-LYSOZYME COMPLEX	[*]

PDB_ID[†]	Description[‡]	Ref
4NLF	2'-TRIFLUOROMETHYLTHIO-2'-DEOXYCYTIDINE-MODIFIED SRL	[*]
4O26	CRYSTAL STRUCTURE OF THE TRBD DOMAIN OF TERT AND THE CR4/5 OF TR	[213]
4PCJ	MODIFICATIONS TO TOXIC CUG RNAS INDUCE STRUCTURAL STABILITY AND RESCUE MIS-SPLICING IN MYOTONIC DYSTROPHY	[214]
4PWD	CRYSTAL STRUCTURE OF HIV-1 REVERSE TRANSCRIPTASE IN COMPLEX WITH BULGE-RNA/DNA AND NEVIRAPINE	[215]
4QIK	CRYSTAL STRUCTURE OF THE ROQ DOMAIN OF HUMAN ROQUIN IN COMPLEX WITH THE TNF23 RNA DUPLEX	[216]
4RZD	CRYSTAL STRUCTURE OF A PREQ1 RIBOSWITCH	[217]
4TS2	CRYSTAL STRUCTURE OF THE SPINACH RNA APTAMER IN COMPLEX WITH DFHBI, MAGNESIUM IONS	[218]
4U7U	CRYSTAL STRUCTURE OF RNA-GUIDED IMMUNE CASCADE COMPLEX FROM E.COLI	[219]
4XWF	CRYSTAL STRUCTURE OF THE ZMP RIBOSWITCH AT 1.80 ANGSTROM	[220]
4Y1J	LACTOCOCCUS LACTIS YYBP-YKOY MN RIBOSWITCH A41U BINDING SITE MUTANT IN PRESENCE OF MN2+	[221]
4Y1M	AN ESCHERICHIA COLI YYBP-YKOY MN RIBOSWITCH IN THE MN2+-FREE STATE	[222]
4YAZ	3',3'-CGAMP RIBOSWITCH BOUND WITH 3',3'-CGAMP	[223]
5AOX	HUMAN ALU RNA RETROTRANSPOSITION COMPLEX IN THE RIBOSOME-STALLING CONFORMATION	[224]
5B2P	CRYSTAL STRUCTURE OF FRANCISELLA NOVICIDA CAS9 IN COMPLEX WITH SGRNA AND TARGET DNA (TGA PAM)	[225]
5B2T	CRYSTAL STRUCTURE OF THE STREPTOCOCCUS PYOGENES CAS9 VRER VARIANT IN COMPLEX WITH SGRNA AND TARGET DNA (TGCG PAM)	[226]
5BTM	CRYSTAL STRUCTURE OF AUUCU REPEATING RNA THAT CAUSES SPINOCEREBELLAR ATAXIA TYPE 10 (SCA10)	[227]
5CZZ	CRYSTAL STRUCTURE OF STAPHYLOCOCCUS AUREUS CAS9 IN COMPLEX WITH SGRNA AND TARGET DNA (TTGAAT PAM)	[*]
5D8H	CRYSTAL STRUCTURE OF THE BASE OF THE RIBOSOMAL P STALK FROM METHANOCOCCUS JANNASCHII WITH ANTIBIOTIC THIOSTREPTON	[*]
5DDP	L-GLUTAMINE RIBOSWITCH BOUND WITH L-GLUTAMINE	[228]
5F5F	X-RAY STRUCTURE OF ROQUIN ROQ DOMAIN IN COMPLEX WITH A SELEX-DERIVED HEXA-LOOP RNA MOTIF	[229]
5F5H	X-RAY STRUCTURE OF ROQUIN ROQ DOMAIN IN COMPLEX WITH OX40 HEXA-LOOP RNA MOTIF	[230]
5F9F	CRYSTAL STRUCTURE OF RIG-I HELICASE-RD IN COMPLEX WITH 24-MER BLUNT-END HAIRPIN RNA	[231]
5FJ4	STRUCTURE OF THE STANDARD KINK TURN HMKT-7 AS STEM LOOP BOUND WITH U1A AND L7AE PROTEINS	[232]
5FJC	SAM-I RIBOSWITCH BEARING THE H. MARISMORTUI KT-7 VARIANT C-2BU	[233]
5FQ5	CRYSTAL STRUCTURE OF CAS9-SGRNA-DNA COMPLEX SOLVED BY NATIVE SAD PHASING	[234]
5G4T	THE STRUCTURE OF A QUASI-CYCLIC SIX K-TURN DUPLEX RNA SPECIES	[235]
5G4U	ASSOCIATION OF THREE TWO-K-TURN UNITS BASED ON KT-7 3BU,3NU, FORMING A TRIANGULAR-SHAPED STRUCTURE	[236]
5HC9	THERMOTOGA MARITIMA CCA-ADDING ENZYME COMPLEXED WITH TRNA_CCA	[237]
5HR6	X-RAY CRYSTAL STRUCTURE OF C118A RLMN WITH CROSS-LINKED TRNA PURIFIED FROM ESCHERICHIA COLI	[238]
5HR7	X-RAY CRYSTAL STRUCTURE OF C118A RLMN FROM ESCHERICHIA COLI WITH CROSS-LINKED IN VITRO TRANSCRIBED TRNA	[239]
5KPY	STRUCTURE OF A 5-HYDROXYTRYPTOPHAN APTAMER	[240]
5LQO	RNA DUPLEX HAS CENTRAL CONSECUTIVE GA PAIRS FLANKED BY G-C BASEPAIRS	[241]
5LQT	RNA DUPLEX HAS CENTRAL CONSECUTIVE GA PAIRS FLANKED BY G-C BASEPAIRS	[242]
5LR3	RNA DUPLEX HAS CENTRAL CONSECUTIVE GA PAIRS FLANKED BY G-U BASEPAIRS	[243]
5M0H	CRYSTAL STRUCTURE OF THE CENTRAL FLEXIBLE REGION OF ASH1 MRNA E3-LOCALIZATION ELEMENT	[244]
5M0J	CRYSTAL STRUCTURE OF THE CYTOPLASMIC COMPLEX WITH SHE2P, SHE3P, AND THE ASH1 MRNA E3-LOCALIZATION ELEMENT	[245]
5T83	STRUCTURE OF A GUANIDINE-I RIBOSWITCH FROM S. ACIDOPHILUS	[246]
5U30	CRYSTAL STRUCTURE OF AACC2C1-SGRNA-EXTENDED TARGET DNA TERNARY COMPLEX	[247]
5UDZ	HUMAN LIN28A IN COMPLEX WITH LET-7F-1 MICRORNA PRE-ELEMENT	[248]
5V1K	STRUCTURE OF R-GNA DODECAMER	[249]

PDB_ID[†]	Description[‡]	Ref
5V3F	CO-CRYSTAL STRUCTURE OF THE FLUOROGENIC RNA MANGO	[250]
5VCI	RNA HAIRPIN STRUCTURE CONTAINING TETRALOOP/RECEPTOR MOTIF, COMPLEXED WITH 2-MEIMPG ANALOGUE	[251]
5WTI	CRYSTAL STRUCTURE OF THE CRISPR-ASSOCIATED PROTEIN IN COMPLEX WITH CRRNA AND DNA	[252]
5X2G	CRYSTAL STRUCTURE OF CAMPYLOBACTER JEJUNI CAS9 IN COMPLEX WITH SGRNA AND TARGET DNA (AGAAACC PAM)	[253]
5Y58	CRYSTAL STRUCTURE OF KU70/80 AND TLC1	[254]
6D3P	CRYSTAL STRUCTURE OF AN EXORIBONUCLEASE-RESISTANT RNA FROM SWEET CLOVER NECROTIC MOSAIC VIRUS (SCNMV)	[255]
	mRNA	
2HW8	STRUCTURE OF RIBOSOMAL PROTEIN L1-MRNA COMPLEX AT 2.1 RESOLUTION.	[256]
3P6Y	CF IM25-CF IM68-UGUAA COMPLEX	[*]
5M0I	CRYSTAL STRUCTURE OF THE NUCLEAR COMPLEX WITH SHE2P AND THE ASH1 MRNA E3-LOCALIZATION ELEMENT	[257]
	Signal recognition particle RNA	
1L9A	CRYSTAL STRUCTURE OF SRP19 IN COMPLEX WITH THE S DOMAIN OF SIGNAL RECOGNITION PARTICLE RNA	[258]
3LQX	SRP RIBONUCLEOPROTEIN CORE COMPLEXED WITH COBALT HEXAMMINE	[259]
3NDB	CRYSTAL STRUCTURE OF A SIGNAL SEQUENCE BOUND TO THE SIGNAL RECOGNITION PARTICLE	[260]
4C7O	THE STRUCTURAL BASIS OF FTSY RECRUITMENT AND GTPASE ACTIVATION BY SRP RNA	[261]
4WFL	STRUCTURE OF THE COMPLETE BACTERIAL SRP ALU DOMAIN	[262]
4ZT0	CRYSTAL STRUCTURE OF CATALYTICALLY-ACTIVE STREPTOCOCCUS PYOGENES CAS9 IN COMPLEX WITH SINGLE-GUIDE RNA AT 2.9 ANGSTROM RESOLUTION	[263]
	Single-stranded RNA	
1Q96	CRYSTAL STRUCTURE OF A MUTANT OF THE SARCIN/RICIN DOMAIN FROM RAT 28S RRNA	[264]
1RLG	MOLECULAR BASIS OF BOX C/D RNA-PROTEIN INTERACTION: CO-CRYSTAL STRUCTURE OF THE ARCHAEAL SRNP INTIATION COMPLEX	[265]
361D	CRYSTAL STRUCTURE OF DOMAIN E OF THERMUS FLAVUS 5S RRNA: A HELICAL RNA-STRUCTURE INCLUDING A TETRALOOP	[266]
3G9Y	CRYSTAL STRUCTURE OF THE SECOND ZINC FINGER FROM ZRANB2/ZNF265 BOUND TO 6 NT SSRNA SEQUENCE AGGUAA	[267]
3MDG	CRYSTAL STRUCTURE OF THE 25KDA SUBUNIT OF HUMAN CLEAVAGE FACTOR IM IN COMPLEX WITH RNA UUGUAU	[268]
3MDI	CRYSTAL STRUCTURE OF THE 25KDA SUBUNIT OF HUMAN CLEAVAGE FACTOR IM IN COMPLEX WITH RNA UGUAAA	[269]
3SIU	STRUCTURE OF A HPRP31-15.5K-U4ATAC 5' STEM LOOP COMPLEX, MONOMERIC FORM	[270]
	Small nuclear RNA	
1E7K	CRYSTAL STRUCTURE OF THE SPLICEOSOMAL 15.5KD PROTEIN BOUND TO A U4 SNRNA FRAGMENT	[271]
6ASO	STRUCTURE OF YEAST U6 SNRNP WITH 3'-PHOSPHATE TERMINATED U6 RNA	[272]
	Telomerase RNA	
4O26	CRYSTAL STRUCTURE OF THE TRBD DOMAIN OF TERT AND THE CR4/5 OF TR	[273]
	Triplex RNA	
3P22	CRYSTAL STRUCTURE OF THE ENE, A VIRAL RNA STABILITY ELEMENT, IN COMPLEX WITH A9 RNA	[274]
	Quadruplex RNA	
6C63	CRYSTAL STRUCTURE OF THE MANGO-II FLUORESCENT APTAMER BOUND TO TO1-BIOTIN	[275]
6C65	CRYSTAL STRUCTURE OF THE MANGO-II-A22U FLUORESCENT APTAMER BOUND TO TO1-BIOTIN	[276]

PDB_ID[†]	Description[‡]	Ref
	Viral RNA	
1L2X	ATOMIC RESOLUTION CRYSTAL STRUCTURE OF A VIRAL RNA PSEUDOKNOT	[277]
1U1Y	CRYSTAL STRUCTURE OF A COMPLEX BETWEEN WT BACTERIOPHAGE MS2 COAT PROTEIN AND AN F5 APTAMER RNA STEMLOOP WITH 2AMINOPURINE SUBSTITUTED AT THE-10 POSITION	[278]
5MSF	MS2 PROTEIN CAPSID/RNA COMPLEX	[279]
5O7H	STRUCTURE OF THE CASCADE-I-FV COMPLEX FROM SHEWANELLA PUTREFACIENS	[280]
	Viral fragement	
1XJR	THE STRUCTURE OF A RIGOROUSLY CONSERVED RNA ELEMENT WITHIN THE SARS VIRUS GENOME	[281]
4PQV	CRYSTAL STRUCTURE OF AN XRN1-RESISTANT RNA FROM THE 3' UNTRANSLATED REGION OF A FLAVIVIRUS (MURRAY VALLEY ENCEPHALITIS VIRUS)	[282]
5TPY	CRYSTAL STRUCTURE OF AN EXONUCLEASE RESISTANT RNA FROM ZIKA VIRUS	[283]
6D3P	CRYSTAL STRUCTURE OF AN EXORIBONUCLEASE-RESISTANT RNA FROM SWEET CLOVER NECROTIC MOSAIC VIRUS (SCNMV)	[284]
	Non-coding RNA	
2XD0	A PROCESSED NON-CODING RNA REGULATES A BACTERIAL ANTIVIRAL SYSTEM	[285]
2XDB	A PROCESSED NON-CODING RNA REGULATES A BACTERIAL ANTIVIRAL SYSTEM	[286]
4ATO	NEW INSIGHTS INTO THE MECHANISM OF BACTERIAL TYPE III TOXIN-ANTITOXIN SYSTEMS: SELECTIVE TOXIN INHIBITION BY A NON-CODING RNA PSEUDOKNOT	[287]
	Other RNA types	
2XLK	CRYSTAL STRUCTURE OF THE CSY4-CRRNA COMPLEX, ORTHORHOMBIC FORM	[288]
4LGT	CRYSTAL STRUCTURE OF THE CATALYTIC DOMAIN OF RLUB IN COMPLEX WITH A 21-NUCLEOTIDE RNA SUBSTRATE	[289]
4RMO	CRYSTAL STRUCTURE OF THE CPTIN TYPE III TOXIN-ANTITOXIN SYSTEM FROM EUBACTERIUM RECTALE	[290]
5L2L	NAB2 ZN FINGERS 5-7 BOUND TO A11G RNA	[291]
5LYS	THE CRYSTAL STRUCTURE OF 7SK 5'-HAIRPIN - GOLD DERIVATIVE	[292]
5WWE	CRYSTAL STRUCTURE OF HNRNPA2B1 IN COMPLEX WITH RNA	[293]
5XTM	CRYSTAL STRUCTURE OF PHORPP38 BOUND TO A K-TURN IN P12.2 HELIX	[294]

[†]PDB_ID refers to the structural identification code used in the Protein Data Bank.[1]

[‡]Classifications taken from the Protein Data Bank[1] and Nucleic Acid Database.[2] The following structures, which belong to two categories, are listed twice: 3EGZ, 3Q50, 3V7E, 4FEN, 4FRG, 4L81, 4M4O, 4O26, 4RZD, 4TS2, 4XWF, 4Y1J, 4Y1M, 4YAZ, 5DDP, 5FJC, 5KPY, 5T83, 6C63, 6C65, 6D3P.

References – Table S1

[1] Shalev-Benami M, Zhang Y, Matzov D, Halfon Y, Zackay A, et al. (2016). 2.8-Å Cryo-EM Structure of the Large Ribosomal Subunit from the Eukaryotic Parasite Leishmania. Cell Rep 16(2): 288-294.

[2] Ben-Shem A, Garreau de Loubresse N, Melnikov S, Jenner L, Yusupova G, et al. (2011). The structure of the eukaryotic ribosome at 3.0 Å resolution. Science 334(6062): 1524-9.

[3] Demeshkina N, Jenner L, Westhof E, Yusupov M, Yusupova G (2012). A new understanding of the decoding principle on the ribosome. Nature 484(7393): 256-9.

[4] Demeshkina N, Jenner L, Westhof E, Yusupov M, Yusupova G (2012). A new understanding of the decoding principle on the ribosome. Nature 484(7393): 256-9.

[5] Chen Y, Feng S, Kumar V, Ero R, Gao YG (2013). Structure of EF-G-ribosome complex in a pretranslocation state. Nat Struct Mol Biol 20(9): 1077-84.

[6] Gabdulkhakov A, Nikonov S, Garber M (2013). Revisiting the Haloarcula marismortui 50S ribosomal subunit model. Acta Crystallogr D Biol Crystallogr 69(Pt 6): 997-1004.

[7] Polikanov YS, Melnikov SV, Söll D, Steitz TA (2015). Structural insights into the role of rRNA modifications in protein synthesis and ribosome assembly. Nat Struct Mol Biol 22(4): 342-344.

[8] Kaminishi T, Schedlbauer A, Fabbretti A, Brandi L, Ochoa-Lizarralde B, et al. (2015). Crystallographic characterization of the ribosomal binding site and molecular mechanism of action of Hygromycin A. Nucleic Acids Res 43(20): 10015-25.

[9] Rozov A, Demeshkina N, Khusainov I, Westhof E, Yusupov M, et al. (2016). Novel base-pairing interactions at the tRNA wobble position crucial for accurate reading of the genetic code. Nat Commun 7: 10457.

[10] Rozov A, Westhof E, Yusupov M, Yusupova G (2016). The ribosome prohibits the G•U wobble geometry at the first position of the codon-anticodon helix. Nucleic Acids Res 44(13): 6434-41.

[11] Matzov D, Aibara S, Basu A, Zimmerman E, Bashan A, et al. (2017). The cryo-EM structure of hibernating 100S ribosome dimer from pathogenic Staphylococcus aureus. Nat Commun 8(1): 723.

[12] Zhang X, Lai M, Chang W, Yu I, Ding K, et al. (2016). Structures and stabilization of kinetoplastid-specific split rRNAs revealed by comparing leishmanial and human ribosomes. Nat Commun 7: 13223.

[13] Liu Z, Gutierrez-Vargas C, Wei J, Grassucci RA, Ramesh M, et al. (2016). Structure and assembly model for the Trypanosoma cruzi 60S ribosomal subunit. Proc Natl Acad Sci U S A 113(43): 12174-12179.

[14] Perez Boerema A, Aibara S, Paul B, Tobiasson V, Kimanius D, et al. (2018). Structure of the chloroplast ribosome with chl-RRF and hibernation-promoting factor. Nat Plants 4(4): 212-217.

[15] Rozov A, Wolff P, Grosjean H, Yusupov M, Yusupova G, et al. (2018). Tautomeric G•U pairs within the molecular ribosomal grip and fidelity of decoding in bacteria. Nucleic Acids Res 46(14): 7425-7435.

[16] Tishchenko S, Gabdulkhakov A, Nevskaya N, Sarskikh A, Kostareva O, et al. (2012). High-resolution crystal structure of the isolated ribosomal L1 stalk. Acta Crystallogr D Biol Crystallogr 68(Pt 8): 1051-7.

[17] Seefeldt AC, Graf M, Pérébaskine N, Nguyen F, Arenz S, et al. (2016). Structure of the mammalian antimicrobial peptide Bac7(1-16) bound within the exit tunnel of a bacterial ribosome. Nucleic Acids Res 44(5): 2429-38.

[18] Rozov A, Westhof E, Yusupov M, Yusupova G (2016). The ribosome prohibits the G•U wobble geometry at the first position of the codon-anticodon helix. Nucleic Acids Res 44(13): 6434-41.

[19] Cocozaki AI, Altman RB, Huang J, Buurman ET, Kazmirski SL, et al. (2016). Resistance mutations generate divergent antibiotic susceptibility profiles against translation inhibitors. Proc Natl Acad Sci U S A 113(29): 8188-93.

[20] Könst ZA, Szklarski AR, Pellegrino S, Michalak SE, Meyer M, et al. (2017). Synthesis facilitates an understanding of the structural basis for translation inhibition by the lissoclimides. Nat Chem 9(11): 1140-1149.

[21] Shalev-Benami M, Zhang Y, Rozenberg H, Nobe Y, Taoka M, et al. (2017). Atomic resolution snapshot of Leishmania ribosome inhibition by the aminoglycoside paromomycin. Nat Commun 8(1): 1589.

[22] Shalev-Benami M, Zhang Y, Rozenberg H, Nobe Y, Taoka M, et al. (2017). Atomic resolution snapshot of Leishmania ribosome inhibition by the aminoglycoside paromomycin. Nat Commun 8(1): 1589.

[23] Tereshchenkov AG, Dobosz-Bartoszek M, Osterman IA, Marks J, Sergeeva VA, et al. (2018). Binding and Action of Amino Acid Analogs of Chloramphenicol upon the Bacterial Ribosome. J Mol Biol 430(6): 842-852.

[24] Natchiar SK, Myasnikov AG, Kratzat H, Hazemann I, Klaholz BP (2017). Visualization of chemical modifications in the human 80S ribosome structure. Nature 551(7681): 472-477.

[25] Lu M, Steitz TA (2000). Structure of Escherichia coli ribosomal protein L25 complexed with a 5S rRNA fragment at 1.8-A resolution. Proc Natl Acad Sci U S A 97(5): 2023-8.

[26] Fedorov R, Meshcheryakov V, Gongadze G, Fomenkova N, Nevskaya N, et al. (2001). Structure of ribosomal protein TL5 complexed with RNA provides new insights into the CTC family of stress proteins. Acta Crystallogr D Biol Crystallogr 57(Pt 7): 968-76.

[27] Agalarov SC, Sridhar Prasad G, Funke PM, Stout CD, Williamson JR (2000). Structure of the S15,S6,S18-rRNA complex: assembly of the 30S ribosome central domain. Science 288(5463): 107-13.

[28] Conn GL, Gittis AG, Lattman EE, Misra VK, Draper DE (2002). A compact RNA tertiary structure contains a buried backbone-K+ complex. J Mol Biol 318(4): 963-73.

[29] Revtovich SV, Nikulin AD, Nikonov SV (2004). Role of N-terminal helix in interaction of ribosomal protein S15 with 16S rRNA. Biochemistry (Mosc) 69(12): 1319-23.

[30] Wimberly BT, Guymon R, McCutcheon JP, White SW, Ramakrishnan V (1999). A detailed view of a ribosomal active site: the structure of the L11-RNA complex. Cell 97(4): 491-502.

[31] Nikulin A, Eliseikina I, Tishchenko S, Nevskaya N, Davydova N, et al. (2003). Structure of the L1 protuberance in the ribosome. Nat Struct Biol 10(2): 104-8.
[32] Pallan PS, Marshall WS, Harp J, Jewett FC 3rd, Wawrzak Z, et al. (2005). Crystal structure of a luteoviral RNA pseudoknot and model for a minimal ribosomal frameshifting motif. Biochemistry 44(34): 11315-22.
[33] Lee TT, Agarwalla S, Stroud RM (2005). A unique RNA Fold in the RumA-RNA-cofactor ternary complex contributes to substrate selectivity and enzymatic function. Cell 120(5): 599-611.
[34] Serganov A, Yuan YR, Pikovskaya O, Polonskaia A, Malinina L, et al. (2004). Structural basis for discriminative regulation of gene expression by adenine- and guanine-sensing mRNAs. Chem Biol 11(12): 1729-41.
[35] Serganov A, Yuan YR, Pikovskaya O, Polonskaia A, Malinina L, et al. (2004). Structural basis for discriminative regulation of gene expression by adenine- and guanine-sensing mRNAs. Chem Biol 11(12): 1729-41.
[36] Serganov A, Polonskaia A, Phan AT, Breaker RR, Patel DJ (2006). Structural basis for gene regulation by a thiamine pyrophosphate-sensing riboswitch. Nature 441(7097): 1167-71.
[37] Gilbert SD, Rambo RP, Van Tyne D, Batey RT (2008). Structure of the SAM-II riboswitch bound to S-adenosylmethionine. Nat Struct Mol Biol 15(2): 177-82.
[38] Schroeder KT, Daldrop P, Lilley DM (2011). RNA tertiary interactions in a riboswitch stabilize the structure of a kink turn. Structure 19(9): 1233-40.
[39] Garst AD, Héroux A, Rambo RP, Batey RT (2008). Crystal structure of the lysine riboswitch regulatory mRNA element. J Biol Chem 283(33): 22347-51.
[40] Thore S, Frick C, Ban N (2008). Structural basis of thiamine pyrophosphate analogues binding to the eukaryotic riboswitch. J Am Chem Soc 130(26): 8116-7.
[41] Serganov A, Huang L, Patel DJ (2008). Structural insights into amino acid binding and gene control by a lysine riboswitch. Nature 455(7217): 1263-7.
[42] Lu C, Smith AM, Fuchs RT, Ding F, Rajashankar K, et al. (2008). Crystal structures of the SAM-III/S(MK) riboswitch reveal the SAM-dependent translation inhibition mechanism. Nat Struct Mol Biol 15(10): 1076-83.
[43] Xiao H, Edwards TE, Ferré-D'Amaré AR (2008). Structural basis for specific, high-affinity tetracycline binding by an in vitro evolved aptamer and artificial riboswitch. Chem Biol 15(10): 1125-37.
[44] Serganov A, Huang L, Patel DJ (2009). Coenzyme recognition and gene regulation by a flavin mononucleotide riboswitch. Nature 458(7235): 233-7.
[45] Delfosse V, Bouchard P, Bonneau E, Dagenais P, Lemay JF, et al. (2010). Riboswitch structure: an internal residue mimicking the purine ligand. Nucleic Acids Res 38(6): 2057-68.
[46] Klein DJ, Edwards TE, Ferré-D'Amaré AR (2009). Cocrystal structure of a class I preQ1 riboswitch reveals a pseudoknot recognizing an essential hypermodified nucleobase. Nat Struct Mol Biol 16(3): 343-4.
[47] Dixon N, Duncan JN, Geerlings T, Dunstan MS, McCarthy JE, et al. (2010). Reengineering orthogonally selective riboswitches. Proc Natl Acad Sci U S A 107(7): 2830-5.
[48] Smith KD, Lipchock SV, Livingston AL, Shanahan CA, Strobel SA (2010). Structural and biochemical determinants of ligand binding by the c-di-GMP riboswitch . Biochemistry 49(34): 7351-9.
[49] Edwards AL, Reyes FE, Héroux A, Batey RT (2010). Structural basis for recognition of S-adenosylhomocysteine by riboswitches. RNA 16(11): 2144-55.
[50] Huang L, Serganov A, Patel DJ (2010). Structural insights into ligand recognition by a sensing domain of the cooperative glycine riboswitch. Mol Cell 40(5): 774-86.
[51] Ramesh A, Wakeman CA, Winkler WC (2011). Insights into metalloregulation by M-box riboswitch RNAs via structural analysis of manganese-bound complexes. J Mol Biol 407(4): 556-70.
[52] Smith KD, Shanahan CA, Moore EL, Simon AC, Strobel SA (2011). Structural basis of differential ligand recognition by two classes of bis-(3'-5')-cyclic dimeric guanosine monophosphate-binding riboswitches. Proc Natl Acad Sci U S A 108(19): 7757-62.
[53] Jenkins JL, Krucinska J, McCarty RM, Bandarian V, Wedekind JE (2011). Comparison of a preQ1 riboswitch aptamer in metabolite-bound and free states with implications for gene regulation. J Biol Chem 286(28): 24626-37.
[54] Buck J, Wacker A, Warkentin E, Wöhnert J, Wirmer-Bartoschek J, et al. (2011). Influence of ground-state structure and Mg2+ binding on folding kinetics of the guanine-sensing riboswitch aptamer domain. Nucleic Acids Res 39(22): 9768-78.
[55] Pikovskaya O, Polonskaia A, Patel DJ, Serganov A (2011). Structural principles of nucleoside selectivity in a 2'-deoxyguanosine riboswitch. Nat Chem Biol 7(10): 748-55.
[56] Pikovskaya O, Polonskaia A, Patel DJ, Serganov A (2011). Structural principles of nucleoside selectivity in a 2'-deoxyguanosine riboswitch. Nat Chem Biol 7(10): 748-55.
[57] Huang L, Ishibe-Murakami S, Patel DJ, Serganov A (2011). Long-range pseudoknot interactions dictate the regulatory response in the tetrahydrofolate riboswitch. Proc Natl Acad Sci U S A 108(36): 14801-6.
[58] Baird NJ, Zhang J, Hamma T, Ferré-D'Amaré AR (2012). YbxF and YlxQ are bacterial homologs of L7Ae and bind K-turns but not K-loops. RNA 18(4): 759-70.
[59] Schroeder KT, Daldrop P, McPhee SA, Lilley DM (2012). Structure and folding of a rare, natural kink turn in RNA with an A*A pair at the 2b*2n position. RNA 18(6): 1257-66.
[60] Ren A, Rajashankar KR, Patel DJ (2012). Fluoride ion encapsulation by Mg2+ ions and phosphates in a fluoride riboswitch. Nature 486(7401): 85-9.

[61] Stoddard CD, Widmann J, Trausch JJ, Marcano-Velázquez JG, Knight R, et al. (2013). Nucleotides adjacent to the ligand-binding pocket are linked to activity tuning in the purine riboswitch. J Mol Biol 425(10): 1596-611.
[62] Johnson JE Jr, Reyes FE, Polaski JT, Batey RT (2012). B12 cofactors directly stabilize an mRNA regulatory switch. Nature 492(7427): 133-7.
[63] Liberman JA, Salim M, Krucinska J, Wedekind JE (2013). Structure of a class II preQ1 riboswitch reveals ligand recognition by a new fold. Nat Chem Biol 9(6): 353-5.
[64] Trausch JJ, Xu Z, Edwards AL, Reyes FE, Ross PE, et al. (2014). Structural basis for diversity in the SAM clan of riboswitches. Proc Natl Acad Sci U S A 111(18): 6624-9.
[65] Trausch JJ, Batey RT (2014). A disconnect between high-affinity binding and efficient regulation by antifolates and purines in the tetrahydrofolate riboswitch. Chem Biol 21(2): 205-16.
[66] Robinson CJ, Vincent HA, Wu MC, Lowe PT, Dunstan MS, et al. (2014). Modular riboswitch toolsets for synthetic genetic control in diverse bacterial species. J Am Chem Soc 136(30): 10615-24.
[67] Ren A, Patel DJ (2014). c-di-AMP binds the ydaO riboswitch in two pseudo-symmetry-related pockets. Nat Chem Biol 10(9): 780-6.
[68] Furukawa K, Ramesh A, Zhou Z, Weinberg Z, Vallery T, et al. (2015). Bacterial riboswitches cooperatively bind Ni(2+) or Co(2+) ions and control expression of heavy metal transporters. Mol Cell 57(6): 1088-1098.
[69] Liberman JA, Suddala KC, Aytenfisu A, Chan D, Belashov IA, et al. (2015). Structural analysis of a class III preQ1 riboswitch reveals an aptamer distant from a ribosome-binding site regulated by fast dynamics. Proc Natl Acad Sci U S A 112(27): E3485-94.
[70] Liu Y, Holmstrom E, Zhang J, Yu P, Wang J, et al. (2015). Synthesis and applications of RNAs with position-selective labelling and mosaic composition. Nature 522(7556): 368-72.
[71] Trausch JJ, Marcano-Velázquez JG, Matyjasik MM, Batey RT (2015). Metal Ion-Mediated Nucleobase Recognition by the ZTP Riboswitch. Chem Biol 22(7): 829-37.
[72] Price IR, Gaballa A, Ding F, Helmann JD, Ke A (2015). Mn(2+)-sensing mechanisms of yybP-ykoY orphan riboswitches. Mol Cell 57(6): 1110-1123.
[73] Price IR, Gaballa A, Ding F, Helmann JD, Ke A (2015). Mn(2+)-sensing mechanisms of yybP-ykoY orphan riboswitches. Mol Cell 57(6): 1110-1123.
[74] Ren A, Wang XC, Kellenberger CA, Rajashankar KR, Jones RA, et al. (2015). Structural basis for molecular discrimination by a 3',3'-cGAMP sensing riboswitch. Cell Rep 11(1): 1-12.
[75] Ren A, Rajashankar KR, Patel DJ (2015). Global RNA Fold and Molecular Recognition for a pfl Riboswitch Bound to ZMP, a Master Regulator of One-Carbon Metabolism. Structure 23(8): 1375-1381.
[76] Howe JA, Wang H, Fischmann TO, Balibar CJ, Xiao L, et al. (2015). Selective small-molecule inhibition of an RNA structural element. Nature 526(7575): 672-7.
[77] Ren A, Xue Y, Peselis A, Serganov A, Al-Hashimi HM, et al. (2015). Structural and Dynamic Basis for Low-Affinity, High-Selectivity Binding of L-Glutamine by the Glutamine Riboswitch. Cell Rep 13(9): 1800-13.
[78] Huang L, Wang J, Lilley DM (2016). A critical base pair in k-turns determines the conformational class adopted, and correlates with biological function. Nucleic Acids Res 44(11): 5390-8.
[79] Huang L, Wang J, Wilson TJ, Lilley DMJ (2017). Structure of the Guanidine III Riboswitch. Cell Chem Biol 24(11): 1407-1415.e2.
[80] Stagno JR, Liu Y, Bhandari YR, Conrad CE, Panja S, et al. (2017). Structures of riboswitch RNA reaction states by mix-and-inject XFEL serial crystallography. Nature 541(7636): 242-246.
[81] Reiss CW, Xiong Y, Strobel SA (2017). Structural Basis for Ligand Binding to the Guanidine-I Riboswitch. Structure 25(1): 195-202.
[82] Battaglia RA, Price IR, Ke A (2017). Structural basis for guanidine sensing by the ykkC family of riboswitches. RNA 23(4): 578-585.
[83] Bachas ST, Ferré-D'Amaré AR (2018). Convergent Use of Heptacoordination for Cation Selectivity by RNA and Protein Metalloregulators. Cell Chem Biol 25(8): 962-973.e5.
[84] Knappenberger AJ, Reiss CW, Strobel SA (2018). Structures of two aptamers with differing ligand specificity reveal ruggedness in the functional landscape of RNA. Elife 7.
[85] Vicens Q, Mondragón E, Reyes FE, Coish P, Aristoff P, et al. (2018). Structure-Activity Relationship of Flavin Analogues That Target the Flavin Mononucleotide Riboswitch. ACS Chem Biol 13(10): 2908-2919.
[86] Huang L, Lilley DMJ (2018). Structure and ligand binding of the SAM-V riboswitch. Nucleic Acids Res 46(13): 6869-6879.
[87] Pley HW, Flaherty KM, McKay DB (1994). Three-dimensional structure of a hammerhead ribozyme. Nature 372(6501): 68-74.
[88] Zhang L, Doudna JA (2002). Structural insights into group II intron catalysis and branch-site selection. Science 295(5562): 2084-8.
[89] Krasilnikov AS, Xiao Y, Pan T, Mondragón A (2004). Basis for structural diversity in homologous RNAs. Science 306(5693): 104-7.
[90] Serganov A, Keiper S, Malinina L, Tereshko V, Skripkin E, et al. (2005). Structural basis for Diels-Alder ribozyme-catalyzed carbon-carbon bond formation. Nat Struct Mol Biol 12(3): 218-24.
[91] Martick M, Lee TS, York DM, Scott WG (2008). Solvent structure and hammerhead ribozyme catalysis. Chem Biol 15(4): 332-42.

[92] Robertson MP, Scott WG (2007). The structural basis of ribozyme-catalyzed RNA assembly. Science 315(5818): 1549-53.
[93] Torelli AT, Krucinska J, Wedekind JE (2007). A comparison of vanadate to a 2'-5' linkage at the active site of a small ribozyme suggests a role for water in transition-state stabilization. RNA 13(7): 1052-70.
[94] Chi YI, Martick M, Lares M, Kim R, Scott WG, et al. (2008). Capturing hammerhead ribozyme structures in action by modulating general base catalysis. PLoS Biol 6(9): e234.
[95] Chi YI, Martick M, Lares M, Kim R, Scott WG, et al. (2008). Capturing hammerhead ribozyme structures in action by modulating general base catalysis. PLoS Biol 6(9): e234.
[96] Ye JD, Tereshko V, Frederiksen JK, Koide A, Fellouse FA, et al. (2008). Synthetic antibodies for specific recognition and crystallization of structured RNA. Proc Natl Acad Sci U S A 105(1): 82-7.
[97] Klein DJ, Wilkinson SR, Been MD, Ferré-D'Amaré AR (2007). Requirement of helix P2.2 and nucleotide G1 for positioning the cleavage site and cofactor of the glmS ribozyme. J Mol Biol 373(1): 178-89.
[98] Feig AL, Scott WG, Uhlenbeck OC (1998). Inhibition of the hammerhead ribozyme cleavage reaction by site-specific binding of Tb. Science 279(5347): 81-4.
[99] MacElrevey C, Salter JD, Krucinska J, Wedekind JE (2008). Structural effects of nucleobase variations at key active site residue Ade38 in the hairpin ribozyme. RNA 14(8): 1600-16.
[100] Xiao H, Murakami H, Suga H, Ferré-D'Amaré AR (2008). Structural basis of specific tRNA aminoacylation by a small in vitro selected ribozyme. Nature 454(7202): 358-61.
[101] Cochrane JC, Lipchock SV, Smith KD, Strobel SA (2009). Structural and chemical basis for glucosamine 6-phosphate binding and activation of the glmS ribozyme. Biochemistry 48(15): 3239-46.
[102] Spitale RC, Volpini R, Heller MG, Krucinska J, Cristalli G, et al. (2009). Identification of an imino group indispensable for cleavage by a small ribozyme. J Am Chem Soc 131(17): 6093-5.
[103] Shechner DM, Grant RA, Bagby SC, Koldobskaya Y, Piccirilli JA, et al. (2009). Crystal structure of the catalytic core of an RNA-polymerase ribozyme. Science 326(5957): 1271-5.
[104] Chen JH, Yajima R, Chadalavada DM, Chase E, Bevilacqua PC, et al. (2010). A 1.9 A crystal structure of the HDV ribozyme precleavage suggests both Lewis acid and general acid mechanisms contribute to phosphodiester cleavage. Biochemistry 49(31): 6508-18.
[105] Marcia M, Pyle AM (2012). Visualizing group II intron catalysis through the stages of splicing. Cell 151(3): 497-507.
[106] Liu Y, Wilson TJ, McPhee SA, Lilley DM (2014). Crystal structure and mechanistic investigation of the twister ribozyme. Nat Chem Biol 10(9): 739-44.
[107] Meyer M, Nielsen H, Oliéric V, Roblin P, Johansen SD, et al. (2014). Speciation of a group I intron into a lariat capping ribozyme. Proc Natl Acad Sci U S A 111(21): 7659-64.
[108] Kapral GJ, Jain S, Noeske J, Doudna JA, Richardson DC, et al. (2014). New tools provide a second look at HDV ribozyme structure, dynamics and cleavage. Nucleic Acids Res 42(20): 12833-46.
[109] Kapral GJ, Jain S, Noeske J, Doudna JA, Richardson DC, et al. (2014). New tools provide a second look at HDV ribozyme structure, dynamics and cleavage. Nucleic Acids Res 42(20): 12833-46.
[110] Ren A, Košutić M, Rajashankar KR, Frener M, Santner T, et al. (2014). In-line alignment and Mg^{2+} coordination at the cleavage site of the env22 twister ribozyme. Nat Commun 5: 5534.
[111] Mir A, Chen J, Robinson K, Lendy E, Goodman J, et al. (2015). Two Divalent Metal Ions and Conformational Changes Play Roles in the Hammerhead Ribozyme Cleavage Reaction. Biochemistry 54(41): 6369-81.
[112] Ren A, Vušurović N, Gebetsberger J, Gao P, Juen M, et al. (2016). Pistol ribozyme adopts a pseudoknot fold facilitating site-specific in-line cleavage. Nat Chem Biol 12(9): 702-8.
[113] Nguyen LA, Wang J, Steitz TA (2017). Crystal structure of Pistol, a class of self-cleaving ribozyme. Proc Natl Acad Sci U S A 114(5): 1021-1026.
[114] Liu Y, Wilson TJ, Lilley DMJ (2017). The structure of a nucleolytic ribozyme that employs a catalytic metal ion. Nat Chem Biol 13(5): 508-513.
[115] Zhang W, Tam CP, Zhou L, Oh SS, Wang J, et al. (2018). Structural Rationale for the Enhanced Catalysis of Nonenzymatic RNA Primer Extension by a Downstream Oligonucleotide. J Am Chem Soc 140(8): 2829-2840.
[116] Pitt JN, Ferré-D'Amaré AR (2009). Structure-guided engineering of the regioselectivity of RNA ligase ribozymes. J Am Chem Soc 131(10): 3532-40.
[117] Pitt JN, Ferré-D'Amaré AR (2009). Structure-guided engineering of the regioselectivity of RNA ligase ribozymes. J Am Chem Soc 131(10): 3532-40.
[118] Eiler S, Dock-Bregeon A, Moulinier L, Thierry JC, Moras D (1999). Synthesis of aspartyl-tRNA(Asp) in Escherichia coli--a snapshot of the second step. EMBO J 18(22): 6532-41.
[119] Jovine L, Djordjevic S, Rhodes D (2000). The crystal structure of yeast phenylalanine tRNA at 2.0 A resolution: cleavage by Mg(2+) in 15-year old crystals. J Mol Biol 301(2): 401-14.
[120] Fukai S, Nureki O, Sekine S, Shimada A, Tao J, et al. (2000). Structural basis for double-sieve discrimination of L-valine from L-isoleucine and L-threonine by the complex of tRNA(Val) and valyl-tRNA synthetase. Cell 103(5): 793-803.
[121] Yaremchuk A, Kriklivyi I, Tukalo M, Cusack S (2002). Class I tyrosyl-tRNA synthetase has a class II mode of cognate tRNA recognition. EMBO J 21(14): 3829-40.

[122] Yaremchuk A, Tukalo M, Grøtli M, Cusack S (2001). A succession of substrate induced conformational changes ensures the amino acid specificity of Thermus thermophilus prolyl-tRNA synthetase: comparison with histidyl-tRNA synthetase. J Mol Biol 309(4): 989-1002.
[123] Moulinier L, Eiler S, Eriani G, Gangloff J, Thierry JC, et al. (2001). The structure of an AspRS-tRNA(Asp) complex reveals a tRNA-dependent control mechanism. EMBO J 20(18): 5290-301.
[124] Kobayashi T, Nureki O, Ishitani R, Yaremchuk A, Tukalo M, et al. (2003). Structural basis for orthogonal tRNA specificities of tyrosyl-tRNA synthetases for genetic code expansion. Nat Struct Biol 10(6): 425-32.
[125] Sekine S, Nureki O, Dubois DY, Bernier S, Chênevert R, et al. (2003). ATP binding by glutamyl-tRNA synthetase is switched to the productive mode by tRNA binding. EMBO J 22(3): 676-88.
[126] Sankaranarayanan R, Dock-Bregeon AC, Romby P, Caillet J, Springer M, et al. (1999). The structure of threonyl-tRNA synthetase-tRNA(Thr) complex enlightens its repressor activity and reveals an essential zinc ion in the active site. Cell 97(3): 371-81.
[127] Silvian LF, Wang J, Steitz TA (1999). Insights into editing from an ile-tRNA synthetase structure with tRNAile and mupirocin. Science 285(5430): 1074-7.
[128] Biou V, Yaremchuk A, Tukalo M, Cusack S (1994). The 2.9 A crystal structure of T. thermophilus seryl-tRNA synthetase complexed with tRNA(Ser). Science 263(5152): 1404-10.
[129] Basavappa R, Sigler PB (1991). The 3 A crystal structure of yeast initiator tRNA: functional implications in initiator/elongator discrimination. EMBO J 10(10): 3105-11.
[130] Yang XL, Otero FJ, Ewalt KL, Liu J, Swairjo MA, et al. (2006). Two conformations of a crystalline human tRNA synthetase-tRNA complex: implications for protein synthesis. EMBO J 25(12): 2919-29.
[131] Tukalo M, Yaremchuk A, Fukunaga R, Yokoyama S, Cusack S (2005). The crystal structure of leucyl-tRNA synthetase complexed with tRNALeu in the post-transfer-editing conformation. Nat Struct Mol Biol 12(10): 923-30.
[132] Nakanishi K, Ogiso Y, Nakama T, Fukai S, Nureki O (2005). Structural basis for anticodon recognition by methionyl-tRNA synthetase. Nat Struct Mol Biol 12(10): 931-2.
[133] Tsunoda M, Kusakabe Y, Tanaka N, Ohno S, Nakamura M, et al. (2007). Structural basis for recognition of cognate tRNA by tyrosyl-tRNA synthetase from three kingdoms. Nucleic Acids Res 35(13): 4289-300.
[134] Fukunaga R, Yokoyama S (2007). Structural insights into the first step of RNA-dependent cysteine biosynthesis in archaea. Nat Struct Mol Biol 14(4): 272-9.
[135] Konno M, Sumida T, Uchikawa E, Mori Y, Yanagisawa T, et al. (2009). Modeling of tRNA-assisted mechanism of Arg activation based on a structure of Arg-tRNA synthetase, tRNA, and an ATP analog (ANP). FEBS J 276(17): 4763-79.
[136] Tanaka Y, Yamagata S, Kitago Y, Yamada Y, Chimnaronk S, et al. (2009). Deduced RNA binding mechanism of ThiI based on structural and binding analyses of a minimal RNA ligand. RNA 15(8): 1498-506.
[137] Ito T, Yokoyama S (2010). Two enzymes bound to one transfer RNA assume alternative conformations for consecutive reactions. Nature 467(7315): 612-6.
[138] Sherrer RL, Araiso Y, Aldag C, Ishitani R, Ho JM, et al. (2011). C-terminal domain of archaeal O-phosphoseryl-tRNA kinase displays large-scale motion to bind the 7-bp D-stem of archaeal tRNA(Sec). Nucleic Acids Res 39(3): 1034-41.
[139] Ganichkin OM, Anedchenko EA, Wahl MC (2011). Crystal structure analysis reveals functional flexibility in the selenocysteine-specific tRNA from mouse. PLoS One 6(5): e20032.
[140] Chopra S, Palencia A, Virus C, Tripathy A, Temple BR, et al. (2013). Plant tumour biocontrol agent employs a tRNA-dependent mechanism to inhibit leucyl-tRNA synthetase. Nat Commun 4: 1417.
[141] Grigg JC, Chen Y, Grundy FJ, Henkin TM, Pollack L, et al. (2013). T box RNA decodes both the information content and geometry of tRNA to affect gene expression. Proc Natl Acad Sci U S A 110(18): 7240-5.
[142] Gong P, Kortus MG, Nix JC, Davis RE, Peersen OB (2013). Structures of coxsackievirus, rhinovirus, and poliovirus polymerase elongation complexes solved by engineering RNA mediated crystal contacts. PLoS One 8(5): e60272.
[143] Colussi TM, Costantino DA, Hammond JA, Ruehle GM, Nix JC, et al. (2014). The structural basis of transfer RNA mimicry and conformational plasticity by a viral RNA. Nature 511(7509): 366-9.
[144] Deng X, Qin X, Chen L, Jia Q, Zhang Y, et al. (2016). Large Conformational Changes of Insertion 3 in Human Glycyl-tRNA Synthetase (hGlyRS) during Catalysis. J Biol Chem 291(11): 5740-52.
[145] Tian Q, Wang C, Liu Y, Xie W (2015). Structural basis for recognition of G-1-containing tRNA by histidyl-tRNA synthetase. Nucleic Acids Res 43(5): 2980-90.
[146] Kimura S, Suzuki T, Chen M, Kato K, Yu J, et al. (2016). Template-dependent nucleotide addition in the reverse (3'-5') direction by Thg1-like protein. Sci Adv 2(3): e1501397.
[147] Jones CP, Ferré-D'Amaré AR (2015). Recognition of the bacterial alarmone ZMP through long-distance association of two RNA subdomains. Nat Struct Mol Biol 22(9): 679-85.
[148] Finer-Moore J, Czudnochowski N, O'Connell JD 3rd, Wang AL, Stroud RM (2015). Crystal Structure of the Human tRNA m(1)A58 Methyltransferase-tRNA(3)(Lys) Complex: Refolding of Substrate tRNA Allows Access to the Methylation Target. J Mol Biol 427(24): 3862-76.
[149] Monestier A, Aleksandrov A, Coureux PD, Panvert M, Mechulam Y, et al. (2017). The structure of an E. coli tRNA_f^{Met} A₁-U₇₂ variant shows an unusual conformation of the A₁-U₇₂ base pair. RNA 23(5): 673-682.

[150] Jiang Y, Yu H, Li F, Cheng L, Zhu L, et al. (2018). Unveiling the structural features that determine the dual methyltransferase activities of Streptococcus pneumoniae RlmCD. PLoS Pathog 14(11): e1007379.
[151] Wang W, Chen X, Wolin SL, Xiong Y (2018). Structural Basis for tRNA Mimicry by a Bacterial Y RNA. Structure 26(12): 1635-1644.e3.
[152] Doxtader KA, Wang P, Scarborough AM, Seo D, Conrad NK, et al. (2018). Structural Basis for Regulation of METTL16, an S-Adenosylmethionine Homeostasis Factor. Mol Cell 71(6): 1001-1011.e4.
[153] Sussman D, Wilson C (2000). A water channel in the core of the vitamin B(12) RNA aptamer. Structure 8(7): 719-27.
[154] Baugh C, Grate D, Wilson C (2000). 2.8 A crystal structure of the malachite green aptamer. J Mol Biol 301(1): 117-28.
[155] Huang DB, Vu D, Cassiday LA, Zimmerman JM, Maher LJ 3rd, et al. (2003). Crystal structure of NF-kappaB (p50)2 complexed to a high-affinity RNA aptamer. Proc Natl Acad Sci U S A 100(16): 9268-73.
[156] Lebars I, Legrand P, Aimé A, Pinaud N, Fribourg S, et al. (2008). Exploring TAR-RNA aptamer loop-loop interaction by X-ray crystallography, UV spectroscopy and surface plasmon resonance. Nucleic Acids Res 36(22): 7146-56.
[157] Xiao H, Edwards TE, Ferré-D'Amaré AR (2008). Structural basis for specific, high-affinity tetracycline binding by an in vitro evolved aptamer and artificial riboswitch. Chem Biol 15(10): 1125-37.
[158] Jenkins JL, Krucinska J, McCarty RM, Bandarian V, Wedekind JE (2011). Comparison of a preQ1 riboswitch aptamer in metabolite-bound and free states with implications for gene regulation. J Biol Chem 286(28): 24626-37.
[159] Baird NJ, Zhang J, Hamma T, Ferré-D'Amaré AR (2012). YbxF and YlxQ are bacterial homologs of L7Ae and bind K-turns but not K-loops. RNA 18(4): 759-70.
[160] Stoddard CD, Widmann J, Trausch JJ, Marcano-Velázquez JG, Knight R, et al. (2013). Nucleotides adjacent to the ligand-binding pocket are linked to activity tuning in the purine riboswitch. J Mol Biol 425(10): 1596-611.
[161] Johnson JE Jr, Reyes FE, Polaski JT, Batey RT (2012). B12 cofactors directly stabilize an mRNA regulatory switch. Nature 492(7427): 133-7.
[162] Huang H, Suslov NB, Li NS, Shelke SA, Evans ME, et al. (2014). A G-quadruplex-containing RNA activates fluorescence in a GFP-like fluorophore. Nat Chem Biol 10(8): 686-91.
[163] Trausch JJ, Xu Z, Edwards AL, Reyes FE, Ross PE, et al. (2014). Structural basis for diversity in the SAM clan of riboswitches. Proc Natl Acad Sci U S A 111(18): 6624-9.
[164] Warner KD, Chen MC, Song W, Strack RL, Thorn A, et al. (2014). Structural basis for activity of highly efficient RNA mimics of green fluorescent protein. Nat Struct Mol Biol 21(8): 658-63.
[165] Porter EB, Polaski JT, Morck MM, Batey RT (2017). Recurrent RNA motifs as scaffolds for genetically encodable small-molecule biosensors. Nat Chem Biol 13(3): 295-301.
[166] Fernandez-Millan P, Autour A, Ennifar E, Westhof E, Ryckelynck M (2017). Crystal structure and fluorescence properties of the iSpinach aptamer in complex with DFHBI. RNA 23(12): 1788-1795.
[167] Trachman RJ 3rd, Abdolahzadeh A, Andreoni A, Cojocaru R, Knutson JR, et al. (2018). Crystal Structures of the Mango-II RNA Aptamer Reveal Heterogeneous Fluorophore Binding and Guide Engineering of Variants with Improved Selectivity and Brightness. Biochemistry 57(26): 3544-3548.
[168] Trachman RJ 3rd, Abdolahzadeh A, Andreoni A, Cojocaru R, Knutson JR, et al. (2018). Crystal Structures of the Mango-II RNA Aptamer Reveal Heterogeneous Fluorophore Binding and Guide Engineering of Variants with Improved Selectivity and Brightness. Biochemistry 57(26): 3544-3548.
[169] Dearborn AD, Eren E, Watts NR, Palmer IW, Kaufman JD, et al. (2018). Structure of an RNA Aptamer that Can Inhibit HIV-1 by Blocking Rev-Cognate RNA (RRE) Binding and Rev-Rev Association. Structure 26(9): 1187-1195.e4.
[170] Ippolito JA, Steitz TA (2000). The structure of the HIV-1 RRE high affinity rev binding site at 1.6 A resolution. J Mol Biol 295(4): 711-7.
[171] Wild K, Weichenrieder O, Leonard GA, Cusack S (1999). The 2 A structure of helix 6 of the human signal recognition particle RNA. Structure 7(11): 1345-52.
[172] Hung LW, Holbrook EL, Holbrook SR (2000). The crystal structure of the Rev binding element of HIV-1 reveals novel base pairing and conformational variability. Proc Natl Acad Sci U S A 97(10): 5107-12.
[173] Yang X, Gérczei T, Glover LT, Correll CC (2001). Crystal structures of restrictocin-inhibitor complexes with implications for RNA recognition and base flipping. Nat Struct Biol 8(11): 968-73.
[174] Deng J, Xiong Y, Pan B, Sundaralingam M (2003). Structure of an RNA dodecamer containing a fragment from SRP domain IV of Escherichia coli. Acta Crystallogr D Biol Crystallogr 59(Pt 6): 1004-11.
[175] Rupert PB, Ferré-D'Amaré AR (2001). Crystal structure of a hairpin ribozyme-inhibitor complex with implications for catalysis. Nature 410(6830): 780-6.
[176] Szép S, Wang J, Moore PB (2003). The crystal structure of a 26-nucleotide RNA containing a hook-turn. RNA 9(1): 44-51.
[177] Jang SB, Baeyens K, Jeong MS, SantaLucia J Jr, Turner D, et al. (2004). Structures of two RNA octamers containing tandem G.A base pairs. Acta Crystallogr D Biol Crystallogr 60(Pt 5): 829-35.
[178] Jang SB, Baeyens K, Jeong MS, SantaLucia J Jr, Turner D, et al. (2004). Structures of two RNA octamers containing tandem G.A base pairs. Acta Crystallogr D Biol Crystallogr 60(Pt 5): 829-35.

[179] Teplova M, Malinina L, Darnell JC, Song J, Lu M, et al. (2011). Protein-RNA and protein-protein recognition by dual KH1/2 domains of the neuronal splicing factor Nova-1. Structure 19(7): 930-44.
[180] Gan J, Tropea JE, Austin BP, Court DL, Waugh DS, et al. (2006). Structural insight into the mechanism of double-stranded RNA processing by ribonuclease III. Cell 124(2): 355-66.
[181] Xue S, Calvin K, Li H (2006). RNA recognition and cleavage by a splicing endonuclease. Science 312(5775): 906-10.
[182] Moroder H, Kreutz C, Lang K, Serganov A, Micura R (2006). Synthesis, oxidation behavior, crystallization and structure of 2'-methylseleno guanosine containing RNAs. J Am Chem Soc 128(30): 9909-18.
[183] Li L, Ye K (2006). Crystal structure of an H/ACA box ribonucleoprotein particle. Nature 443(7109): 302-7.
[184] Gan J, Shaw G, Tropea JE, Waugh DS, Court DL, et al. (2008). A stepwise model for double-stranded RNA processing by ribonuclease III. Mol Microbiol 67(1): 143-54.
[185] Kondo J, Hainrichson M, Nudelman I, Shallom-Shezifi D, Barbieri CM, et al. (2007). Differential selectivity of natural and synthetic aminoglycosides towards the eukaryotic and prokaryotic decoding A sites. Chembiochem 8(14): 1700-9.
[186] Hermann T, Tereshko V, Skripkin E, Patel DJ (None). Apramycin recognition by the human ribosomal decoding site. Blood Cells Mol Dis 38(3): 193-8.
[187] Hermann T, Tereshko V, Skripkin E, Patel DJ (None). Apramycin recognition by the human ribosomal decoding site. Blood Cells Mol Dis 38(3): 193-8.
[188] Liu S, Li P, Dybkov O, Nottrott S, Hartmuth K, et al. (2007). Binding of the human Prp31 Nop domain to a composite RNA-protein platform in U4 snRNP. Science 316(5821): 115-20.
[189] Tishchenko S, Kljashtorny V, Kostareva O, Nevskaya N, Nikulin A, et al. (2008). Domain II of Thermus thermophilus ribosomal protein L1 hinders recognition of its mRNA. J Mol Biol 383(2): 301-5.
[190] Correll CC, Freeborn B, Moore PB, Steitz TA (1997). Metals, motifs, and recognition in the crystal structure of a 5S rRNA domain. Cell 91(5): 705-12.
[191] Correll CC, Freeborn B, Moore PB, Steitz TA (1997). Metals, motifs, and recognition in the crystal structure of a 5S rRNA domain. Cell 91(5): 705-12.
[192] Nomura Y, Sugiyama S, Sakamoto T, Miyakawa S, Adachi H, et al. (2010). Conformational plasticity of RNA for target recognition as revealed by the 2.15 A crystal structure of a human IgG-aptamer complex. Nucleic Acids Res 38(21): 7822-9.
[193] Pallan PS, Kreutz C, Bosio S, Micura R, Egli M (2008). Effects of N2,N2-dimethylguanosine on RNA structure and stability: crystal structure of an RNA duplex with tandem m2 2G:A pairs. RNA 14(10): 2125-35.
[194] Tu C, Tropea JE, Austin BP, Court DL, Waugh DS, et al. (2009). Structural basis for binding of RNA and cofactor by a KsgA methyltransferase. Structure 17(3): 374-85.
[195] Tu C, Tropea JE, Austin BP, Court DL, Waugh DS, et al. (2009). Structural basis for binding of RNA and cofactor by a KsgA methyltransferase. Structure 17(3): 374-85.
[196] Duan J, Li L, Lu J, Wang W, Ye K (2009). Structural mechanism of substrate RNA recruitment in H/ACA RNA-guided pseudouridine synthase. Mol Cell 34(4): 427-39.
[197] Liang B, Zhou J, Kahen E, Terns RM, Terns MP, et al. (2009). Structure of a functional ribonucleoprotein pseudouridine synthase bound to a substrate RNA. Nat Struct Mol Biol 16(7): 740-6.
[198] Perederina A, Esakova O, Quan C, Khanova E, Krasilnikov AS (2010). Eukaryotic ribonucleases P/MRP: the crystal structure of the P3 domain. EMBO J 29(4): 761-9.
[199] Hardin JW, Hu YX, McKay DB (2010). Structure of the RNA binding domain of a DEAD-box helicase bound to its ribosomal RNA target reveals a novel mode of recognition by an RNA recognition motif. J Mol Biol 402(2): 412-27.
[200] Zhou J, Liang B, Li H (2011). Structural and functional evidence of high specificity of Cbf5 for ACA trinucleotide. RNA 17(2): 244-50.
[201] Xue S, Wang R, Yang F, Terns RM, Terns MP, et al. (2010). Structural basis for substrate placement by an archaeal box C/D ribonucleoprotein particle. Mol Cell 39(6): 939-49.
[202] Xue S, Wang R, Yang F, Terns RM, Terns MP, et al. (2010). Structural basis for substrate placement by an archaeal box C/D ribonucleoprotein particle. Mol Cell 39(6): 939-49.
[203] Tu C, Zhou X, Tarasov SG, Tropea JE, Austin BP, et al. (2011). The Era GTPase recognizes the GAUCACCUCC sequence and binds helix 45 near the 3' end of 16S rRNA. Proc Natl Acad Sci U S A 108(25): 10156-61.
[204] Teplova M, Wohlbold L, Khin NW, Izaurralde E, Patel DJ (2011). Structure-function studies of nucleocytoplasmic transport of retroviral genomic RNA by mRNA export factor TAP. Nat Struct Mol Biol 18(9): 990-8.
[205] Kondo J (2012). A structural basis for the antibiotic resistance conferred by an A1408G mutation in 16S rRNA and for the antiprotozoal activity of aminoglycosides. Angew Chem Int Ed Engl 51(2): 465-8.
[206] Nam Y, Chen C, Gregory RI, Chou JJ, Sliz P (2011). Molecular basis for interaction of let-7 microRNAs with Lin28. Cell 147(5): 1080-91.
[207] Haurwitz RE, Sternberg SH, Doudna JA (2012). Csy4 relies on an unusual catalytic dyad to position and cleave CRISPR RNA. EMBO J 31(12): 2824-32.
[208] Huang L, Lilley DM (2013). The molecular recognition of kink-turn structure by the L7Ae class of proteins. RNA 19(12): 1703-10.

[209] Huang L, Lilley DM (2014). Structure of a rare non-standard sequence k-turn bound by L7Ae protein. Nucleic Acids Res 42(7): 4734-40.
[210] Niewoehner O, Jinek M, Doudna JA (2014). Evolution of CRISPR RNA recognition and processing by Cas6 endonucleases. Nucleic Acids Res 42(2): 1341-53.
[211] Niewoehner O, Jinek M, Doudna JA (2014). Evolution of CRISPR RNA recognition and processing by Cas6 endonucleases. Nucleic Acids Res 42(2): 1341-53.
[212] Shalev M, Kondo J, Kopelyanskiy D, Jaffe CL, Adir N, et al. (2013). Identification of the molecular attributes required for aminoglycoside activity against Leishmania. Proc Natl Acad Sci U S A 110(33): 13333-8.
[213] Huang J, Brown AF, Wu J, Xue J, Bley CJ, et al. (2014). Structural basis for protein-RNA recognition in telomerase. Nat Struct Mol Biol 21(6): 507-12.
[214] deLorimier E, Coonrod LA, Copperman J, Taber A, Reister EE, et al. (2014). Modifications to toxic CUG RNAs induce structural stability, rescue mis-splicing in a myotonic dystrophy cell model and reduce toxicity in a myotonic dystrophy zebrafish model. Nucleic Acids Res 42(20): 12768-78.
[215] Das K, Martinez SE, Bandwar RP, Arnold E (2014). Structures of HIV-1 RT-RNA/DNA ternary complexes with dATP and nevirapine reveal conformational flexibility of RNA/DNA: insights into requirements for RNase H cleavage. Nucleic Acids Res 42(12): 8125-37.
[216] Tan D, Zhou M, Kiledjian M, Tong L (2014). The ROQ domain of Roquin recognizes mRNA constitutive-decay element and double-stranded RNA. Nat Struct Mol Biol 21(8): 679-85.
[217] Liberman JA, Suddala KC, Aytenfisu A, Chan D, Belashov IA, et al. (2015). Structural analysis of a class III preQ1 riboswitch reveals an aptamer distant from a ribosome-binding site regulated by fast dynamics. Proc Natl Acad Sci U S A 112(27): E3485-94.
[218] Warner KD, Chen MC, Song W, Strack RL, Thorn A, et al. (2014). Structural basis for activity of highly efficient RNA mimics of green fluorescent protein. Nat Struct Mol Biol 21(8): 658-63.
[219] Zhao H, Sheng G, Wang J, Wang M, Bunkoczi G, et al. (2014). Crystal structure of the RNA-guided immune surveillance Cascade complex in Escherichia coli. Nature 515(7525): 147-50.
[220] Trausch JJ, Marcano-Velázquez JG, Matyjasik MM, Batey RT (2015). Metal Ion-Mediated Nucleobase Recognition by the ZTP Riboswitch. Chem Biol 22(7): 829-37.
[221] Price IR, Gaballa A, Ding F, Helmann JD, Ke A (2015). Mn(2+)-sensing mechanisms of yybP-ykoY orphan riboswitches. Mol Cell 57(6): 1110-1123.
[222] Price IR, Gaballa A, Ding F, Helmann JD, Ke A (2015). Mn(2+)-sensing mechanisms of yybP-ykoY orphan riboswitches. Mol Cell 57(6): 1110-1123.
[223] Ren A, Wang XC, Kellenberger CA, Rajashankar KR, Jones RA, et al. (2015). Structural basis for molecular discrimination by a 3',3'-cGAMP sensing riboswitch. Cell Rep 11(1): 1-12.
[224] Ahl V, Keller H, Schmidt S, Weichenrieder O (2015). Retrotransposition and Crystal Structure of an Alu RNP in the Ribosome-Stalling Conformation. Mol Cell 60(5): 715-727.
[225] Hirano H, Gootenberg JS, Horii T, Abudayyeh OO, Kimura M, et al. (2016). Structure and Engineering of Francisella novicida Cas9. Cell 164(5): 950-61.
[226] Hirano S, Nishimasu H, Ishitani R, Nureki O (2016). Structural Basis for the Altered PAM Specificities of Engineered CRISPR-Cas9. Mol Cell 61(6): 886-94.
[227] Park H, González ÀL, Yildirim I, Tran T, Lohman JR, et al. (2015). Crystallographic and Computational Analyses of AUUCU Repeating RNA That Causes Spinocerebellar Ataxia Type 10 (SCA10). Biochemistry 54(24): 3851-9.
[228] Ren A, Xue Y, Peselis A, Serganov A, Al-Hashimi HM, et al. (2015). Structural and Dynamic Basis for Low-Affinity, High-Selectivity Binding of L-Glutamine by the Glutamine Riboswitch. Cell Rep 13(9): 1800-13.
[229] Janowski R, Heinz GA, Schlundt A, Wommelsdorf N, Brenner S, et al. (2016). Roquin recognizes a non-canonical hexaloop structure in the 3'-UTR of Ox40. Nat Commun 7: 11032.
[230] Janowski R, Heinz GA, Schlundt A, Wommelsdorf N, Brenner S, et al. (2016). Roquin recognizes a non-canonical hexaloop structure in the 3'-UTR of Ox40. Nat Commun 7: 11032.
[231] Devarkar SC, Wang C, Miller MT, Ramanathan A, Jiang F, et al. (2016). Structural basis for m7G recognition and 2'-O-methyl discrimination in capped RNAs by the innate immune receptor RIG-I. Proc Natl Acad Sci U S A 113(3): 596-601.
[232] Huang L, Wang J, Lilley DM (2016). A critical base pair in k-turns determines the conformational class adopted, and correlates with biological function. Nucleic Acids Res 44(11): 5390-8.
[233] Huang L, Wang J, Lilley DM (2016). A critical base pair in k-turns determines the conformational class adopted, and correlates with biological function. Nucleic Acids Res 44(11): 5390-8.
[234] Olieric V, Weinert T, Finke AD, Anders C, Li D, et al. (2016). Data-collection strategy for challenging native SAD phasing. Acta Crystallogr D Struct Biol 72(Pt 3): 421-9.
[235] Huang L, Lilley DM (2016). A quasi-cyclic RNA nano-scale molecular object constructed using kink turns. Nanoscale 8(33): 15189-95.
[236] Huang L, Lilley DM (2016). A quasi-cyclic RNA nano-scale molecular object constructed using kink turns. Nanoscale 8(33): 15189-95.
[237] Yamashita S, Tomita K (2016). Mechanism of 3'-Matured tRNA Discrimination from 3'-Immature tRNA by Class-II CCA-Adding Enzyme. Structure 24(6): 918-25.

[238] Schwalm EL, Grove TL, Booker SJ, Boal AK (2016). Crystallographic capture of a radical S-adenosylmethionine enzyme in the act of modifying tRNA. Science 352(6283): 309-12.
[239] Schwalm EL, Grove TL, Booker SJ, Boal AK (2016). Crystallographic capture of a radical S-adenosylmethionine enzyme in the act of modifying tRNA. Science 352(6283): 309-12.
[240] Porter EB, Polaski JT, Morck MM, Batey RT (2017). Recurrent RNA motifs as scaffolds for genetically encodable small-molecule biosensors. Nat Chem Biol 13(3): 295-301.
[241] Huang L, Ashraf S, Wang J, Lilley DM (2017). Control of box C/D snoRNP assembly by N⁶-methylation of adenine. EMBO Rep 18(9): 1631-1645.
[242] Huang L, Ashraf S, Wang J, Lilley DM (2017). Control of box C/D snoRNP assembly by N⁶-methylation of adenine. EMBO Rep 18(9): 1631-1645.
[243] Huang L, Ashraf S, Wang J, Lilley DM (2017). Control of box C/D snoRNP assembly by N⁶-methylation of adenine. EMBO Rep 18(9): 1631-1645.
[244] Edelmann FT, Schlundt A, Heym RG, Jenner A, Niedner-Boblenz A, et al. (2017). Molecular architecture and dynamics of ASH1 mRNA recognition by its mRNA-transport complex. Nat Struct Mol Biol 24(2): 152-161.
[245] Edelmann FT, Schlundt A, Heym RG, Jenner A, Niedner-Boblenz A, et al. (2017). Molecular architecture and dynamics of ASH1 mRNA recognition by its mRNA-transport complex. Nat Struct Mol Biol 24(2): 152-161.
[246] Reiss CW, Xiong Y, Strobel SA (2017). Structural Basis for Ligand Binding to the Guanidine-I Riboswitch. Structure 25(1): 195-202.
[247] Yang H, Gao P, Rajashankar KR, Patel DJ (2016). PAM-Dependent Target DNA Recognition and Cleavage by C2c1 CRISPR-Cas Endonuclease. Cell 167(7): 1814-1828.e12.
[248] Wang L, Nam Y, Lee AK, Yu C, Roth K, et al. (2017). LIN28 Zinc Knuckle Domain Is Required and Sufficient to Induce let-7 Oligouridylation. Cell Rep 18(11): 2664-2675.
[249] Schlegel MK, Foster DJ, Kel'in AV, Zlatev I, Bisbe A, et al. (2017). Chirality Dependent Potency Enhancement and Structural Impact of Glycol Nucleic Acid Modification on siRNA. J Am Chem Soc 139(25): 8537-8546.
[250] Trachman RJ 3rd, Demeshkina NA, Lau MWL, Panchapakesan SSS, Jeng SCY, et al. (2017). Structural basis for high-affinity fluorophore binding and activation by RNA Mango. Nat Chem Biol 13(7): 807-813.
[251] Zhang W, Tam CP, Zhou L, Oh SS, Wang J, et al. (2018). Structural Rationale for the Enhanced Catalysis of Nonenzymatic RNA Primer Extension by a Downstream Oligonucleotide. J Am Chem Soc 140(8): 2829-2840.
[252] Wu D, Guan X, Zhu Y, Ren K, Huang Z (2017). Structural basis of stringent PAM recognition by CRISPR-C2c1 in complex with sgRNA. Cell Res 27(5): 705-708.
[253] Yamada M, Watanabe Y, Gootenberg JS, Hirano H, Ran FA, et al. (2017). Crystal Structure of the Minimal Cas9 from Campylobacter jejuni Reveals the Molecular Diversity in the CRISPR-Cas9 Systems. Mol Cell 65(6): 1109-1121.e3.
[254] Chen H, Xue J, Churikov D, Hass EP, Shi S, et al. (2018). Structural Insights into Yeast Telomerase Recruitment to Telomeres. Cell 172(1-2): 331-343.e13.
[255] Steckelberg AL, Akiyama BM, Costantino DA, Sit TL, Nix JC, et al. (2018). A folded viral noncoding RNA blocks host cell exoribonucleases through a conformationally dynamic RNA structure. Proc Natl Acad Sci U S A 115(25): 6404-6409.
[256] Tishchenko S, Nikonova E, Nikulin A, Nevskaya N, Volchkov S, et al. (2006). Structure of the ribosomal protein L1-mRNA complex at 2.1 A resolution: common features of crystal packing of L1-RNA complexes. Acta Crystallogr D Biol Crystallogr 62(Pt 12): 1545-54.
[257] Edelmann FT, Schlundt A, Heym RG, Jenner A, Niedner-Boblenz A, et al. (2017). Molecular architecture and dynamics of ASH1 mRNA recognition by its mRNA-transport complex. Nat Struct Mol Biol 24(2): 152-161.
[258] Oubridge C, Kuglstatter A, Jovine L, Nagai K (2002). Crystal structure of SRP19 in complex with the S domain of SRP RNA and its implication for the assembly of the signal recognition particle. Mol Cell 9(6): 1251-61.
[259] Batey RT, Doudna JA (2002). Structural and energetic analysis of metal ions essential to SRP signal recognition domain assembly. Biochemistry 41(39): 11703-10.
[260] Hainzl T, Huang S, Meriläinen G, Brännström K, Sauer-Eriksson AE (2011). Structural basis of signal-sequence recognition by the signal recognition particle. Nat Struct Mol Biol 18(3): 389-91.
[261] Voigts-Hoffmann F, Schmitz N, Shen K, Shan SO, Ataide SF, et al. (2013). The structural basis of FtsY recruitment and GTPase activation by SRP RNA. Mol Cell 52(5): 643-54.
[262] Kempf G, Wild K, Sinning I (2014). Structure of the complete bacterial SRP Alu domain. Nucleic Acids Res 42(19): 12284-94.
[263] Jiang F, Zhou K, Ma L, Gressel S, Doudna JA (2015). STRUCTURAL BIOLOGY. A Cas9-guide RNA complex preorganized for target DNA recognition. Science 348(6242): 1477-81.
[264] Correll CC, Beneken J, Plantinga MJ, Lubbers M, Chan YL (2003). The common and the distinctive features of the bulged-G motif based on a 1.04 A resolution RNA structure. Nucleic Acids Res 31(23): 6806-18.
[265] Moore T, Zhang Y, Fenley MO, Li H (2004). Molecular basis of box C/D RNA-protein interactions; cocrystal structure of archaeal L7Ae and a box C/D RNA. Structure 12(5): 807-18.
[266] Perbandt M, Nolte A, Lorenz S, Bald R, Betzel C, et al. (1998). Crystal structure of domain E of Thermus flavus 5S rRNA: a helical RNA structure including a hairpin loop. FEBS Lett 429(2): 211-5.
[267] Loughlin FE, Mansfield RE, Vaz PM, McGrath AP, Setiyaputra S, et al. (2009). The zinc fingers of the SR-like protein ZRANB2 are single-stranded RNA-binding domains that recognize 5' splice site-like sequences. Proc Natl Acad Sci U S A 106(14): 5581-6.

[268] Yang Q, Gilmartin GM, Doublié S (2010). Structural basis of UGUA recognition by the Nudix protein CFI(m)25 and implications for a regulatory role in mRNA 3' processing. Proc Natl Acad Sci U S A 107(22): 10062-7.
[269] Yang Q, Gilmartin GM, Doublié S (2010). Structural basis of UGUA recognition by the Nudix protein CFI(m)25 and implications for a regulatory role in mRNA 3' processing. Proc Natl Acad Sci U S A 107(22): 10062-7.
[270] Liu S, Ghalei H, Lührmann R, Wahl MC (2011). Structural basis for the dual U4 and U4atac snRNA-binding specificity of spliceosomal protein hPrp31. RNA 17(9): 1655-63.
[271] Vidovic I, Nottrott S, Hartmuth K, Lührmann R, Ficner R (2000). Crystal structure of the spliceosomal 15.5kD protein bound to a U4 snRNA fragment. Mol Cell 6(6): 1331-42.
[272] Montemayor EJ, Didychuk AL, Yake AD, Sidhu GK, Brow DA, et al. (2018). Architecture of the U6 snRNP reveals specific recognition of 3'-end processed U6 snRNA. Nat Commun 9(1): 1749.
[273] Huang J, Brown AF, Wu J, Xue J, Bley CJ, et al. (2014). Structural basis for protein-RNA recognition in telomerase. Nat Struct Mol Biol 21(6): 507-12.
[274] Mitton-Fry RM, DeGregorio SJ, Wang J, Steitz TA, Steitz JA (2010). Poly(A) tail recognition by a viral RNA element through assembly of a triple helix. Science 330(6008): 1244-7.
[275] Trachman RJ 3rd, Abdolahzadeh A, Andreoni A, Cojocaru R, Knutson JR, et al. (2018). Crystal Structures of the Mango-II RNA Aptamer Reveal Heterogeneous Fluorophore Binding and Guide Engineering of Variants with Improved Selectivity and Brightness. Biochemistry 57(26): 3544-3548.
[276] Trachman RJ 3rd, Abdolahzadeh A, Andreoni A, Cojocaru R, Knutson JR, et al. (2018). Crystal Structures of the Mango-II RNA Aptamer Reveal Heterogeneous Fluorophore Binding and Guide Engineering of Variants with Improved Selectivity and Brightness. Biochemistry 57(26): 3544-3548.
[277] Egli M, Minasov G, Su L, Rich A (2002). Metal ions and flexibility in a viral RNA pseudoknot at atomic resolution. Proc Natl Acad Sci U S A 99(7): 4302-7.
[278] Horn WT, Convery MA, Stonehouse NJ, Adams CJ, Liljas L, et al. (2004). The crystal structure of a high affinity RNA stem-loop complexed with the bacteriophage MS2 capsid: further challenges in the modeling of ligand-RNA interactions. RNA 10(11): 1776-82.
[279] Rowsell S, Stonehouse NJ, Convery MA, Adams CJ, Ellington AD, et al. (1998). Crystal structures of a series of RNA aptamers complexed to the same protein target. Nat Struct Biol 5(11): 970-5.
[280] Pausch P, Müller-Esparza H, Gleditzsch D, Altegoer F, Randau L, et al. (2017). Structural Variation of Type I-F CRISPR RNA Guided DNA Surveillance. Mol Cell 67(4): 622-632.e4.
[281] Robertson MP, Igel H, Baertsch R, Haussler D, Ares M Jr, et al. (2005). The structure of a rigorously conserved RNA element within the SARS virus genome. PLoS Biol 3(1): e5.
[282] Chapman EG, Costantino DA, Rabe JL, Moon SL, Wilusz J, et al. (2014). The structural basis of pathogenic subgenomic flavivirus RNA (sfRNA) production. Science 344(6181): 307-10.
[283] Akiyama BM, Laurence HM, Massey AR, Costantino DA, Xie X, et al. (2016). Zika virus produces noncoding RNAs using a multi-pseudoknot structure that confounds a cellular exonuclease. Science 354(6316): 1148-1152.
[284] Steckelberg AL, Akiyama BM, Costantino DA, Sit TL, Nix JC, et al. (2018). A folded viral noncoding RNA blocks host cell exoribonucleases through a conformationally dynamic RNA structure. Proc Natl Acad Sci U S A 115(25): 6404-6409.
[285] Blower TR, Pei XY, Short FL, Fineran PC, Humphreys DP, et al. (2011). A processed noncoding RNA regulates an altruistic bacterial antiviral system. Nat Struct Mol Biol 18(2): 185-90.
[286] Blower TR, Pei XY, Short FL, Fineran PC, Humphreys DP, et al. (2011). A processed noncoding RNA regulates an altruistic bacterial antiviral system. Nat Struct Mol Biol 18(2): 185-90.
[287] Short FL, Pei XY, Blower TR, Ong SL, Fineran PC, et al. (2013). Selectivity and self-assembly in the control of a bacterial toxin by an antitoxic noncoding RNA pseudoknot. Proc Natl Acad Sci U S A 110(3): E241-9.
[288] Haurwitz RE, Jinek M, Wiedenheft B, Zhou K, Doudna JA (2010). Sequence- and structure-specific RNA processing by a CRISPR endonuclease. Science 329(5997): 1355-8.
[289] Czudnochowski N, Ashley GW, Santi DV, Alian A, Finer-Moore J, et al. (2014). The mechanism of pseudouridine synthases from a covalent complex with RNA, and alternate specificity for U2605 versus U2604 between close homologs. Nucleic Acids Res 42(3): 2037-48.
[290] Rao F, Short FL, Voss JE, Blower TR, Orme AL, et al. (2015). Co-evolution of quaternary organization and novel RNA tertiary interactions revealed in the crystal structure of a bacterial protein-RNA toxin-antitoxin system. Nucleic Acids Res 43(19): 9529-40.
[291] Aibara S, Gordon JM, Riesterer AS, McLaughlin SH, Stewart M (2017). Structural basis for the dimerization of Nab2 generated by RNA binding provides insight into its contribution to both poly(A) tail length determination and transcript compaction in Saccharomyces cerevisiae. Nucleic Acids Res 45(3): 1529-1538.
[292] Martinez-Zapien D, Legrand P, McEwen AG, Proux F, Cragnolini T, et al. (2017). The crystal structure of the 5' functional domain of the transcription riboregulator 7SK. Nucleic Acids Res 45(6): 3568-3579.
[293] Wu B, Su S, Patil DP, Liu H, Gan J, et al. (2018). Molecular basis for the specific and multivariant recognitions of RNA substrates by human hnRNP A2/B1. Nat Commun 9(1): 420.
[294] Oshima K, Gao X, Hayashi S, Ueda T, Nakashima T, et al. (2018). Crystal structures of the archaeal RNase P protein Rpp38 in complex with RNA fragments containing a K-turn motif. Acta Crystallogr F Struct Biol Commun 74(Pt 1): 57-64.
[*] To be published

Table S2. Identities and structural features of selected G·A base pairs.

This table — found in the accompanying MS Excel document of the same name — includes Protein Data Bank and DSSR identifiers of the guanine and adenine that comprise the 3256 G·A base pairs in this survey, the six rigid-body parameters describing the spatial arrangement of each G·A pair, the secondary structural context of the individual bases, the identities and lengths of the hydrogen bonds stabilizing each pair, and relevant literature references.

Table S3. Pairing Motifs and Identifiers of Illustrated G·A Pairs.

Images in main text

Figure	Motif	PDB_ID	Chain ID	Base ID
2a	m–M	2z75	B·B	G114···A117
2b	W–W	4y4o	A·A	G629···A611
2c	m+m	2hw8	H·H	G13···A28
2d	m–m	4qlm	A·A	G68···A45
2e	m+W	1yfg	A·A	G57···A20
2f	m–W	5ngm	AA·AA	G457···A435
5a	m–W_{II}	5fjc	A·A	G30···A61
	m–M_{I}	1dfu	M·N	G98···A78
5b	W–W	4v88	A6·A6	G816···A855
	m–$W_{}$	3jcs	2·2	G1435···A1438
5c	W–M	1g1x	I·I	G591···A594
	m–M_{II}	4y4o	A·A	G1077···A1080
5d	m–m	5j7l	BA·BA	G102···A151
	m–W_{I}	5j7l	BA·BA	G113···A353
6a	m–M	5j7l	DA·DA	G2857···A2860
	m+m	5j7l	DA·DA	G1750···A2860
	WC	5j7l	DA·DA	G1750···C1708
6b	m–M	5j7l	DA·DA	G2890···A2810
	m+m	5j7l	DA·DA	G2631···A2810
	WC	5j7l	DA·DA	G2631···C2787
6c	m–M	5j7l	DA·DA	G2595···A2598
	m+W	5j7l	DA·DA	G2436···A2598
	WC	5j7l	DA·DA	G2436···C2073
	Hoogsteen	5j7l	DA·DA	G2436···U2245
6d	m–M	5j7l	DA·DA	G585···A1254
	m–m	5j7l	DA·DA	G808···A1254
	WC	5j7l	DA·DA	G808···C672
6e	m–M	5j7l	DA·DA	G733···A699
	m–W	5j7l	DA·DA	G1633···A699
6f	WC	5j7l	DA·DA	G319···C323
	m–W	5j7l	DA·DA	G319···A299
	.–M	5j7l	DA·DA	G338···A299
	m–M	5j7l	DA·DA	G338···A324

Table S3. Pairing Motifs and Identifiers of Illustrated G·A Pairs – continued.

Images in supplementary materials

Figure	Motif	PDB_ID	Chain ID	Base ID
S4a	m–m	4y4o	A·A	G113···A353
	m–W_I	4y4o	A·A	G430···A262
	m–W_{II}	4y4o	A·A	G391···A373
	m–M	4y4o	A·A	G297···A300
S4b	m+m	4v88	A6·A6	G386···A425
	m+W_I	4v88	A5·A5	G2134···A913
	m+W_{II}	4v88	A5·A5	G616···A3274
	m+M	4v88	A5·A5	G2261···A2262
	W+W	4v88	A5·A5	G2645···A1047
	W+M	4v88	A5·A5	G2677···A2680
	M+M	4y4o	A·A	G428···A415
	M+W	4v88	A5·A5	G518···A572
S7	m–M	3f2q	X·X	G19···A90
S10a	m–M	5j7l	BA·BA	G357···A55
S10b	m–W_{II}	4v88	A2·A2	G461···A446

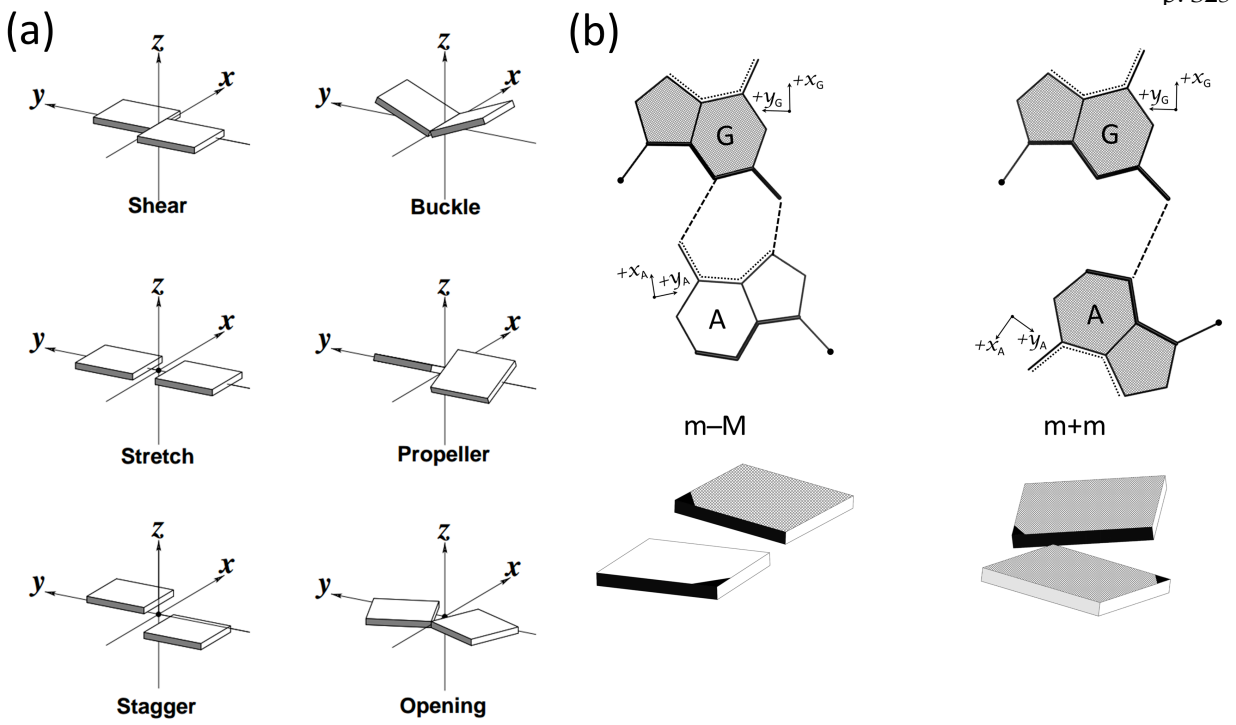

Figure S1. (a) Block depictions of the rigid-body parameters used to describe the spatial arrangements of noncanonical G·A base pairs, here displaying positive values of each parameter.[3] The illustrated reference frames are the average or mid frames between the frames of the individual bases. (b) Base reference frames are constructed such that the positive *x*-axis points away from the minor-groove (thickened/shaded) edge of the base or associated block and the positive *y*-axis away from the Watson-Crick edge.[4] Major-groove atoms with positive values of *x* are highlighted by the finely dotted lines. Left: antiparallel m–M arrangement of G and A with opposing (gray vs. white) faces and directions of base coordinate frames. Right: parallel m+M arrangement with base-pair faces and coordinate frames of the same sense. Black dots on bases and darkened corners on blocks denote the C1´atoms on the attached sugars. Thin dashed lines show hydrogen bonding.

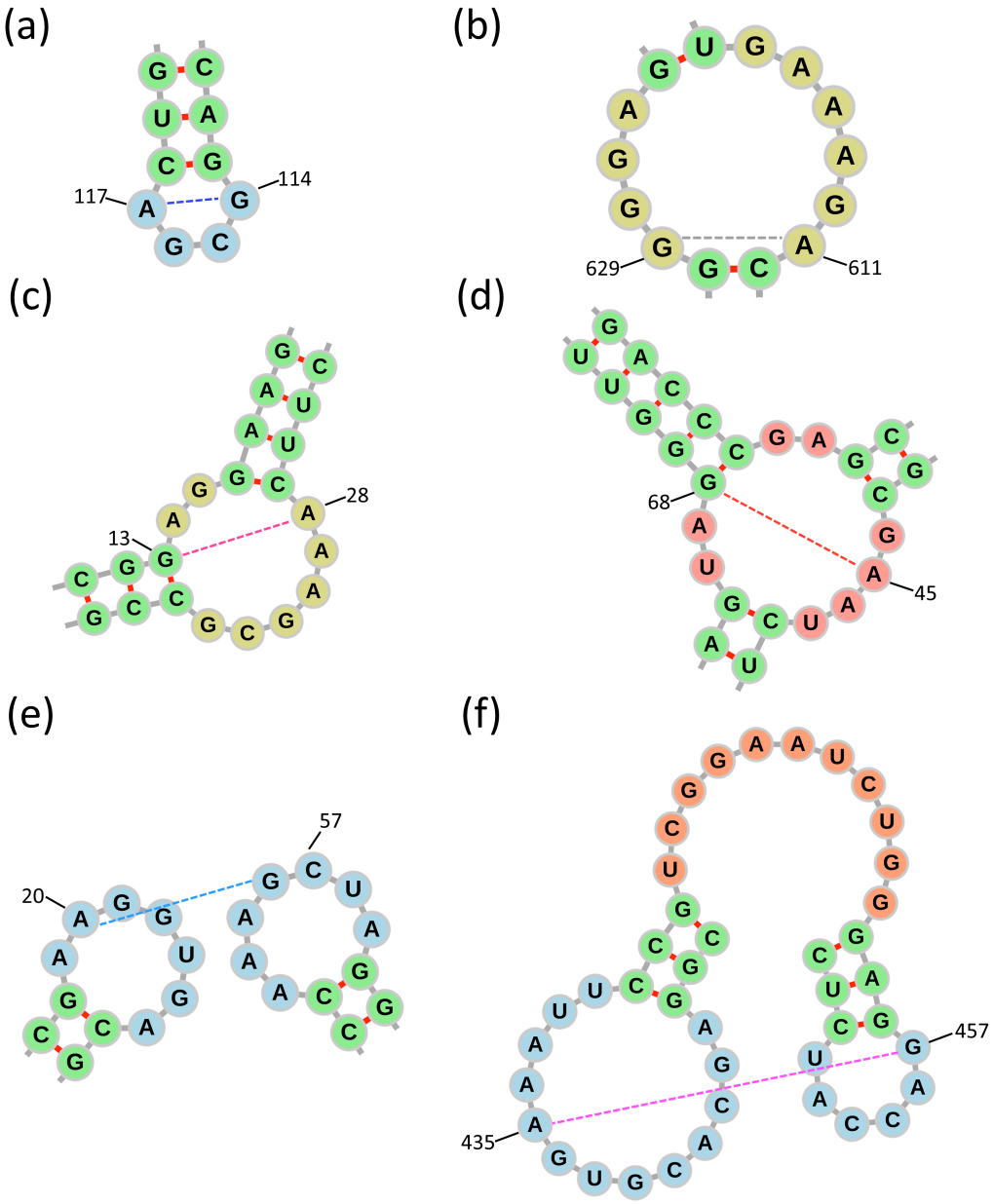

Figure S2. Simple secondary structural diagrams of the three-dimensional motifs incorporating the different modes of G·A base paring shown in Figure 2. Images are constructed using the DSSR-generated dot-bracket representation of the corresponding nucleotides[5] within the force-directed rna (forna) visualization software.[6] The guanine and adenine in each example are denoted by residue number and connected by a dashed line color-coded by the G·A pairing mode used in Figures 1, 2. Canonical Watson-Crick (A–U, G–C) and wobble (G–U) pairs are connected by pink bars and the sugar-phosphate backbones of successive nucleotides are represented by light gray bars. RNA stems, hairpin loops, internal loops (or bulges), and junctions are depicted respectively in green, blue, beige, and magenta.

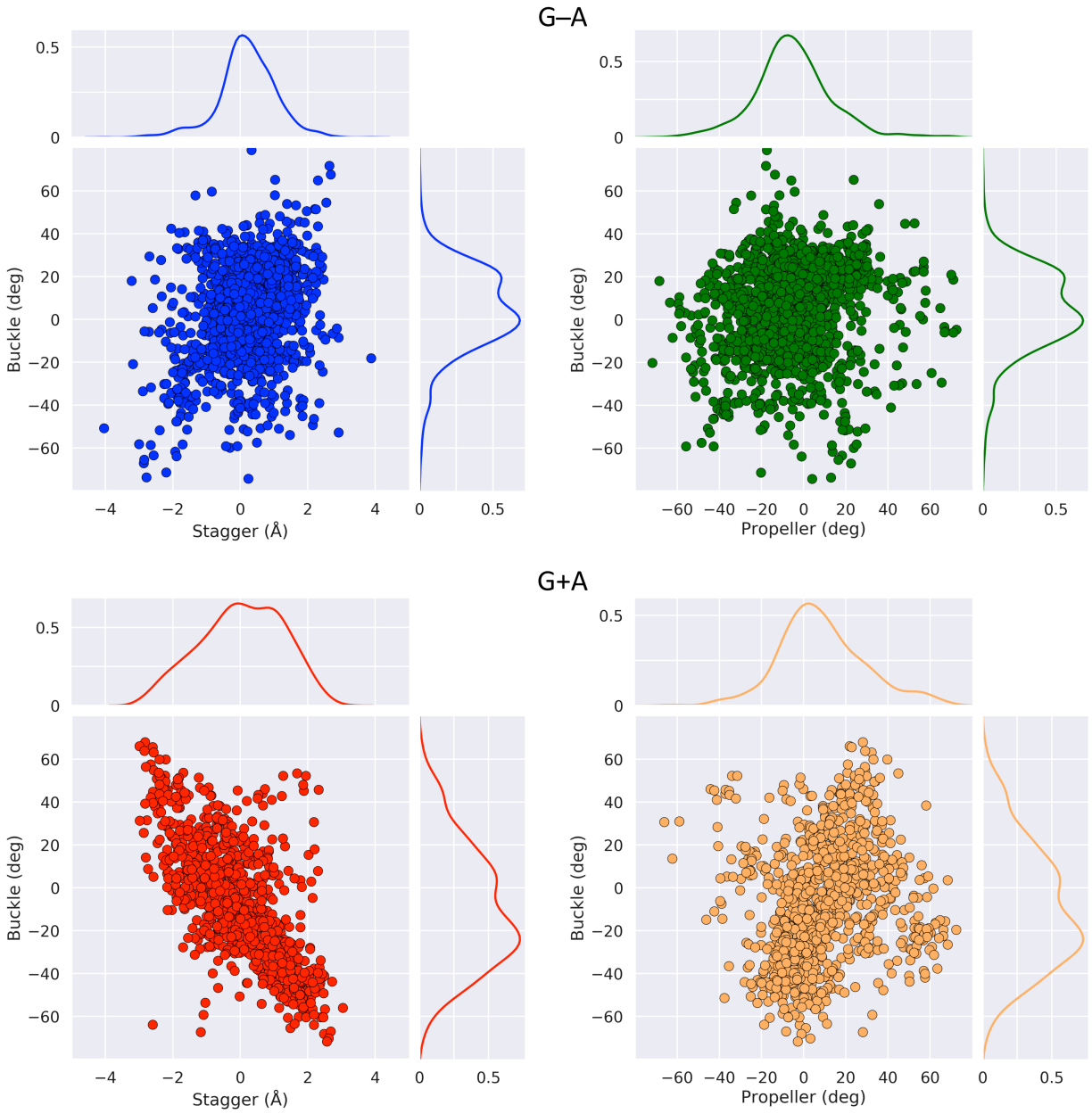

Figure S3. Scatter plots of the rigid-body components — Stagger, Buckle, Propeller — that contribute to G·A non-planarity in RNA-containing crystal structures. Smooth curves on the edges of the scatter plots (Buckle-Stagger at left, Buckle-Propeller at right) are the normalized densities of individual parameters. Images in top row correspond to antiparallel (G–A) arrangements of the two bases and those in the lower row to parallel (G+A) arrangements.

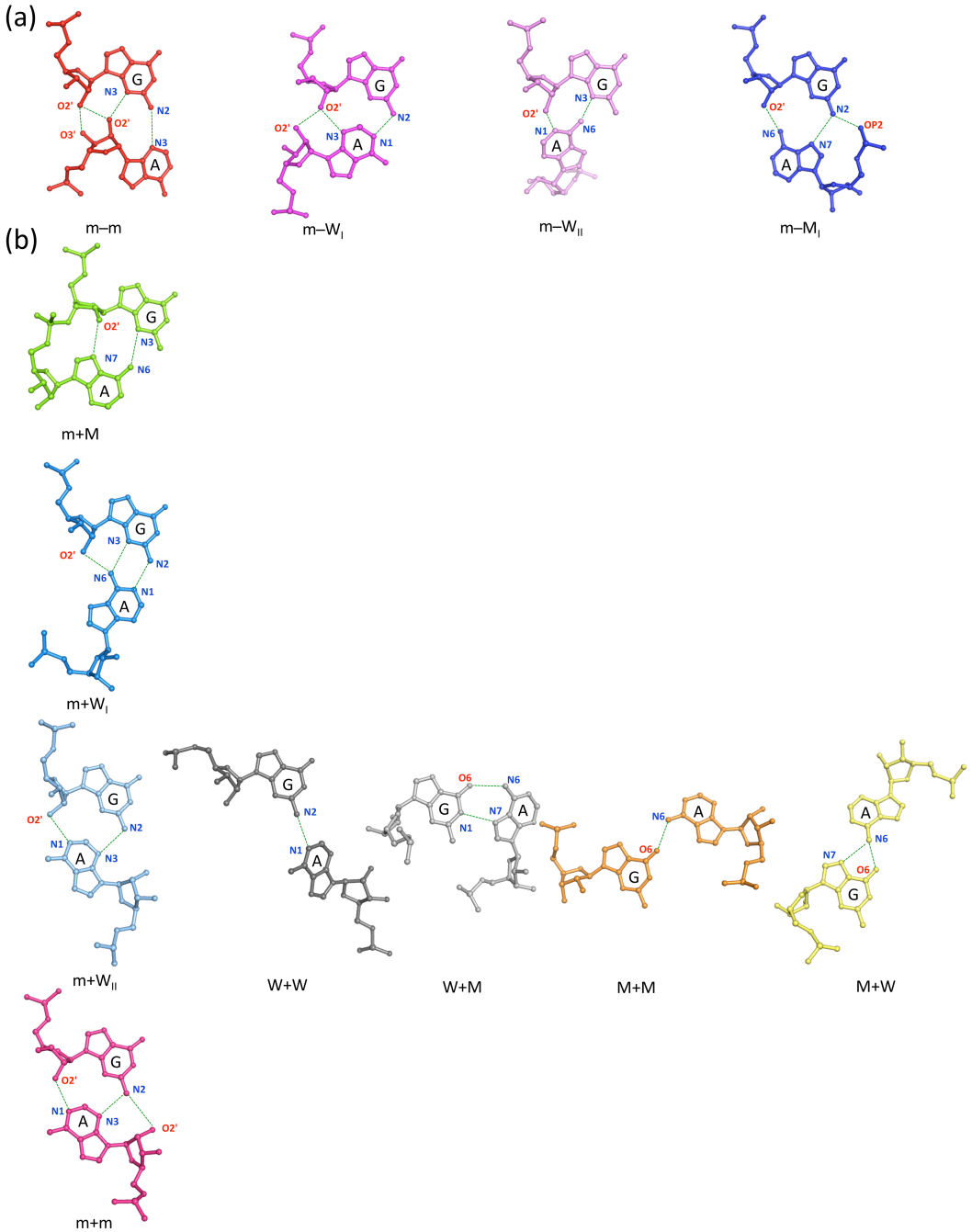

Figure S4. Molecular images illustrating the hydrogen bonds (dashed lines) that link different modes of G·A pairing: (a) the O2´-anchored pathway connecting m–m, m–W_I, m–W_{II}, m–M_I states found in the complex of the *Thermus thermophilus* 70S ribosome with the hibernation factor pY;[7] (b) the three-way connection between m+m, m+W_I, m+M and W+W, W+M, M+M, M+W arrangements of G and A states via the m+W_{II} form found in the aforementioned structure[7] and in the 80S *Saccharomyces cerevisiae* ribosome.[8] See Table S3 for respective Protein Data Bank identifiers, chain names, and residue numbers of depicted G·A pairs. G·A color-coding matches that in Figures 1 and 2.

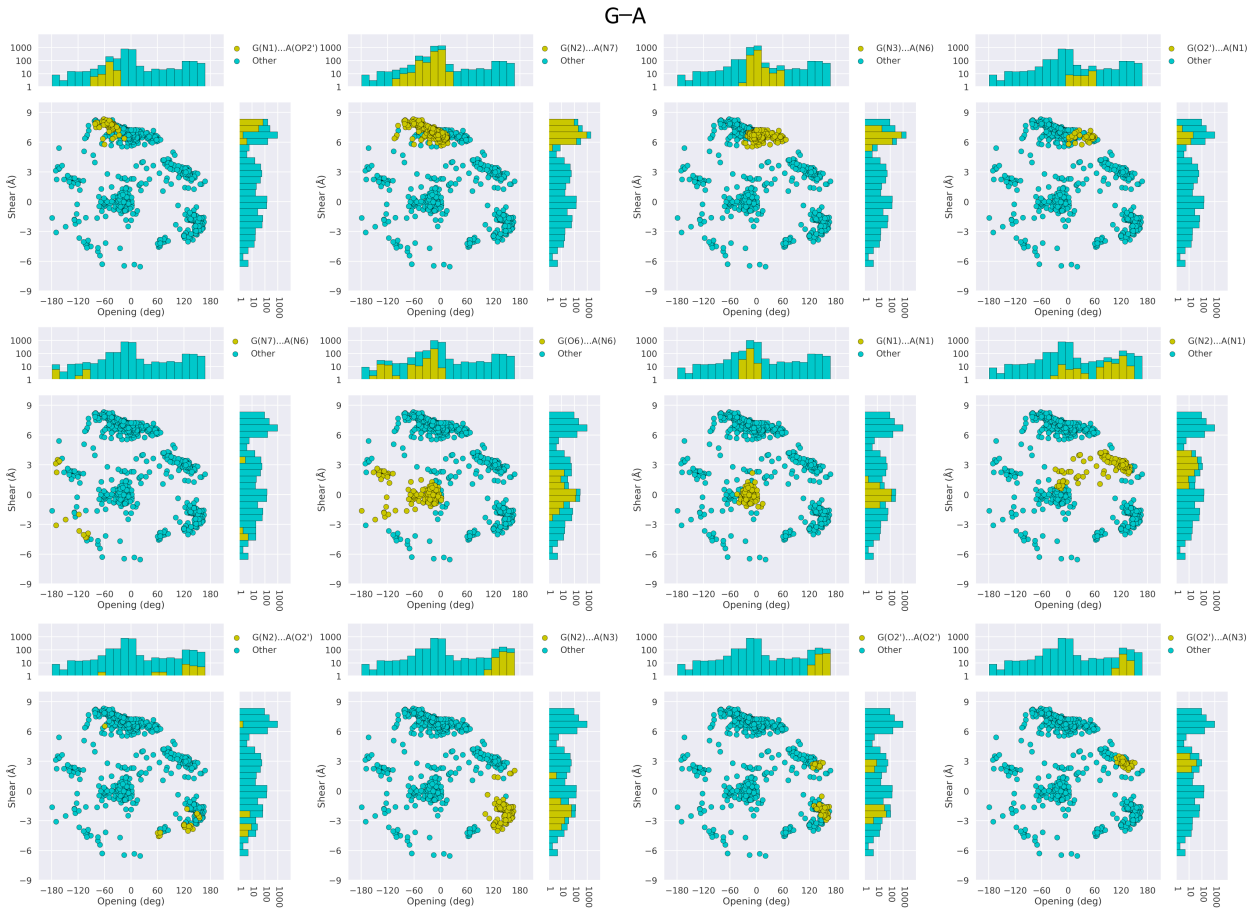

Figure S5. (a) Scatter plots of Shear and Opening in antiparallel G–A base pairs color-coded by hydrogen bonding. Individual images show the arrangements of bases that accommodate each of 16 types of hydrogen bonding (gold points). Comparison of the images with the corresponding plots in Figure 3 reveals the patterns of atomic interactions preserved in related pairing modes, e.g., the G(O6)···A(N6) donor-acceptor pairs highlighted in the second scatter plot in the second row of the grid coincide with G·A pairs labeled W–W, M–W, M–M in Figure 3. Histograms on the edges of the scatter plots depict the spread of hydrogen bonding (gold bars) along individual components. Counts reported on a logarithmic scale.

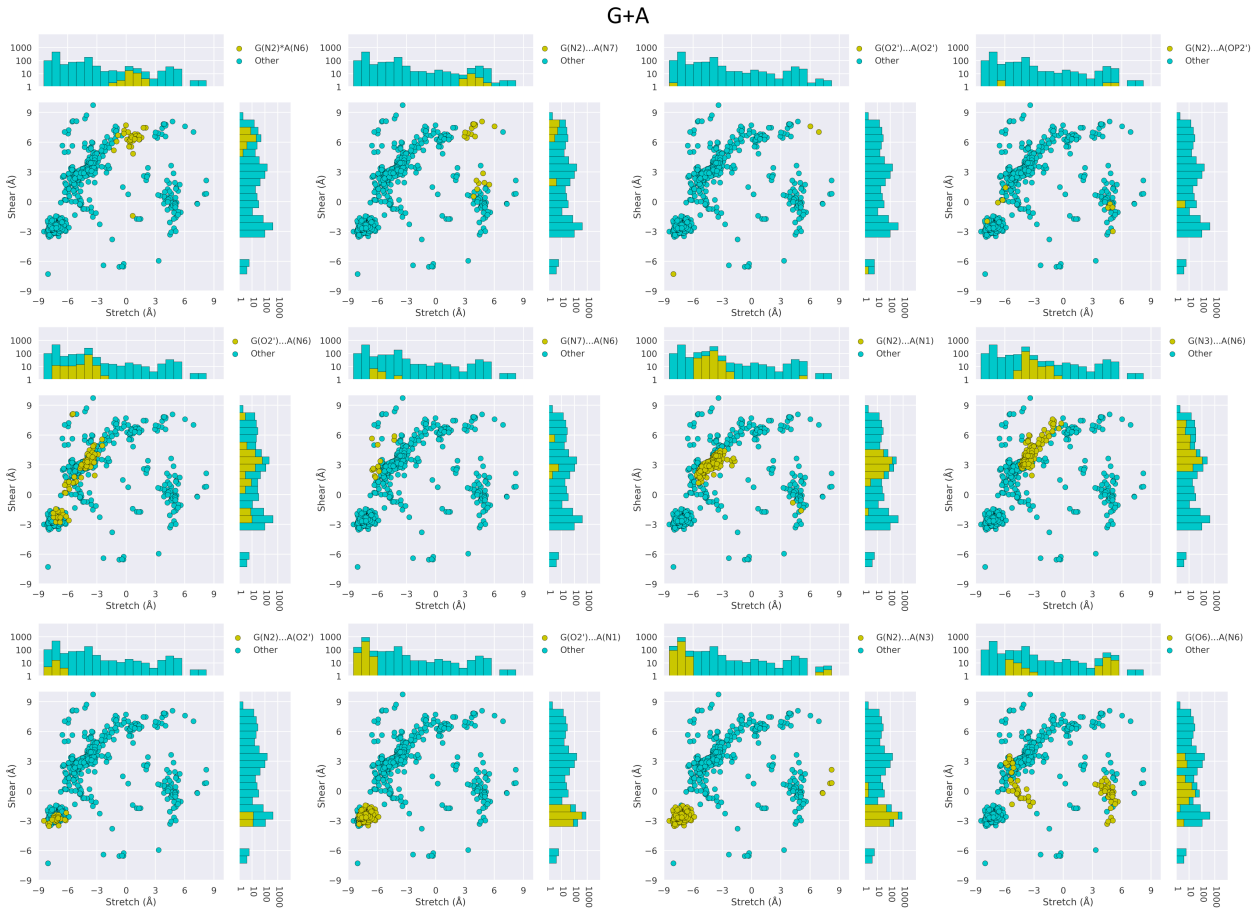

Figure S5. (b) Scatter plots of Shear and Stretch in parallel G+A base pairs color-coded by hydrogen bonding. Individual images show the arrangements of bases that accommodate each of 16 types of hydrogen bonding (gold points). Comparison of the images with the corresponding plots in Figure 3 reveals the patterns of atomic interactions preserved in related pairing modes (see example in the legend to Figure 4a). Histograms on the edges of the scatter plots depict the spread of hydrogen bonding (gold bars) along individual components. Counts reported on a logarithmic scale.

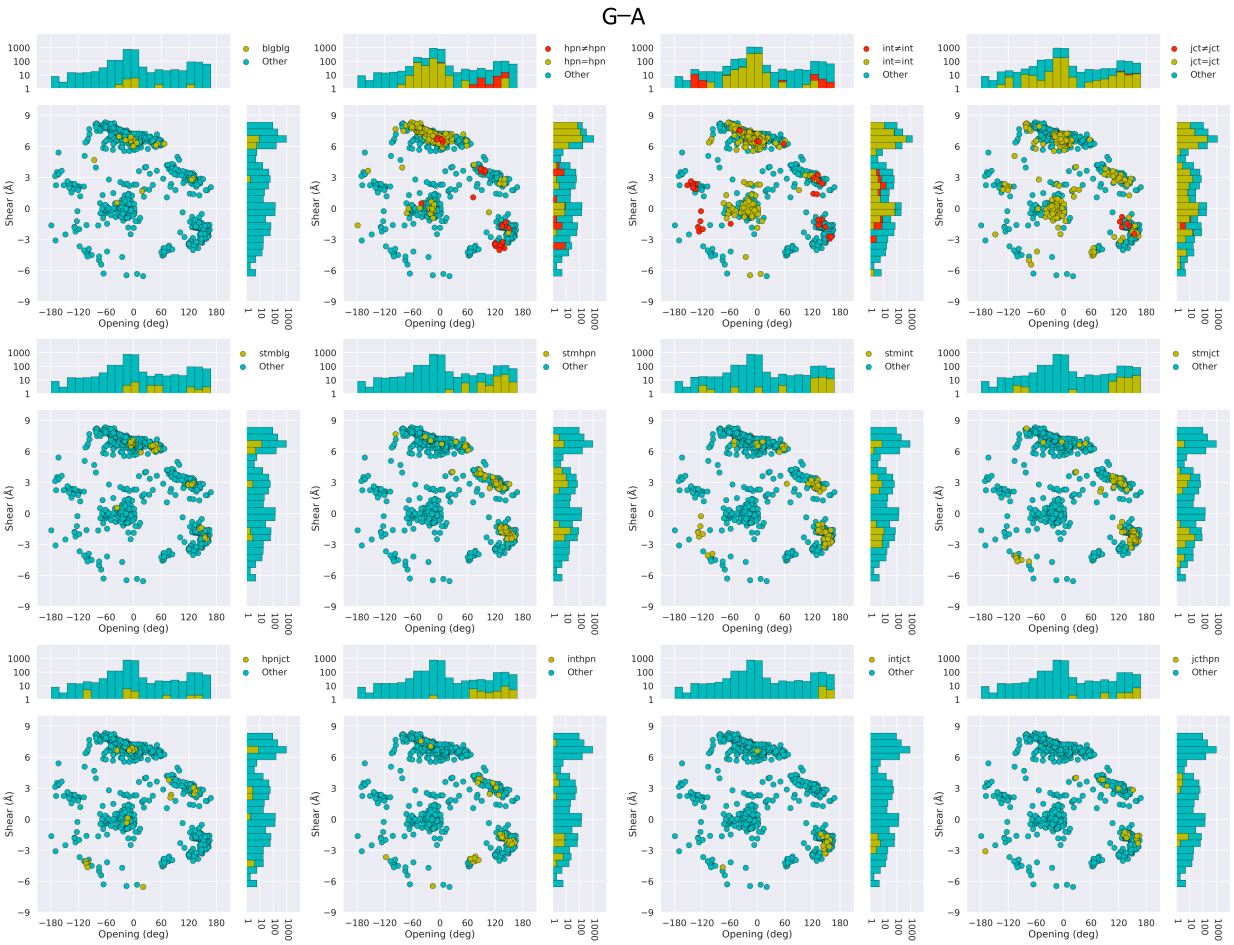

Figure S6. (a) Scatter plots of Shear and Opening in antiparallel G–A base pairs color-coded by secondary structural context. Individual images show the arrangements of bases found in each of 16 combinations of secondary structural elements (gold, red points). Comparison of the images with the corresponding plots in Figure 3 reveals the preferred higher-order organization of the different pairing modes. Points labeled in terms of the secondary structural context of guanine followed by that of adenine: blg – bulge loop; hpn – hairpin loop; int – internal loop; jct – junction loop; stm – canonical double-helical stem. Signs designate whether the base pair occurs in the same (=) or a different (≠) structural element, e.g., hpn≠hpn denotes a pair linking the G and A in different hairpin loops.

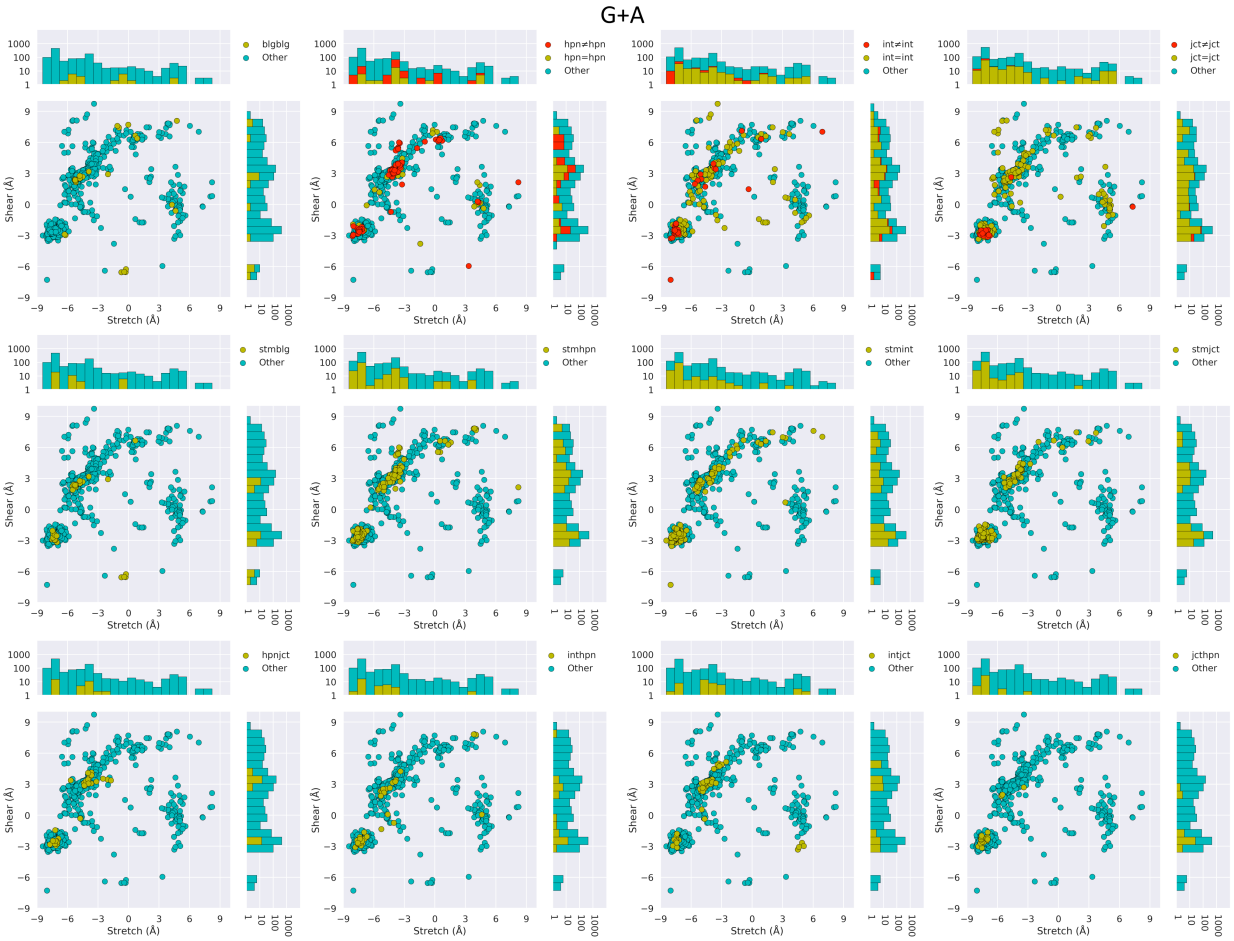

Figure S6. (b) Scatter plots of Shear and Stretch in parallel G+A base pairs color-coded by secondary structural context. Individual images show the arrangements of bases found in each of 16 combinations of secondary structural elements (gold, red points). Comparison of the images with the corresponding plots in Figure 3 reveals the preferred higher-order organization of the different pairing modes. Points labeled in terms of the secondary structural context of guanine followed by that of adenine: blg – bulge loop; hpn – hairpin loop; int – internal loop; jct – junction loop; stm – canonical double-helical stem. Signs designate whether the base pair occurs in the same (=) or a different (≠) structural element, e.g., hpn≠hpn denotes a pair linking the G and A in different hairpin loops.

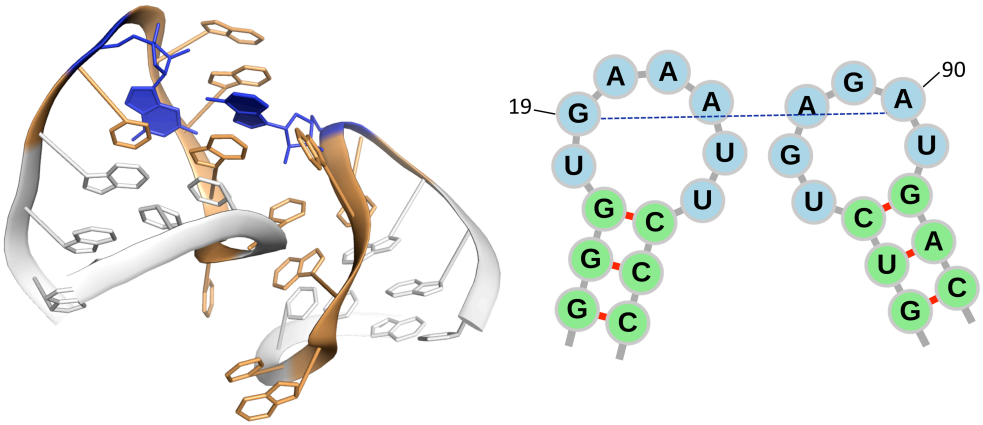

Figure S7. Molecular image (left) and simple secondary structural diagram (right) of an unusual m–M sheared G·A pair linking a guanine and an adenine in different hairpin loops of the flavin mononucleotide riboswitch.[9] The adenine forms an intercalating interaction with the nucleotides in the associated G-containing loop along the lines of the long-range tertiary interactions predicted by Jaeger et al.[10] See Table S3 for the Protein Data Bank identifier, chain names, and residue numbers of the illustrated pair and Figure S2 for further details of the secondary structural diagram. G·A color-coding matches that in Figures 1, 2.

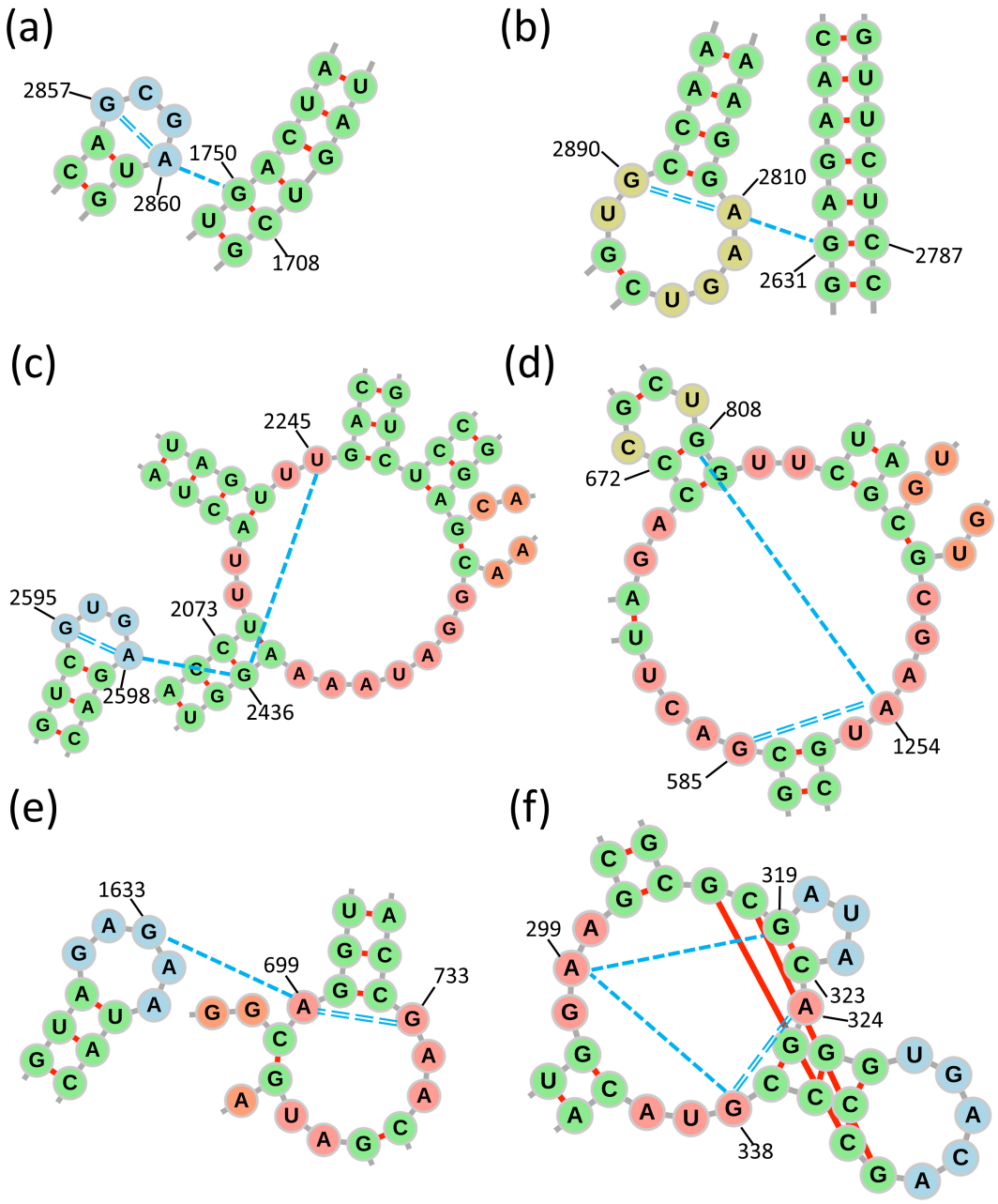

Figure S8. Simple secondary structural diagrams of the three-dimensional motifs incorporating the G·A-mediated multiplets shown in Figure 6. Images are constructed using the DSSR-generated dot-bracket representation of the corresponding nucleotides[5] within the force-directed rna (forna) visualization software.[6] The paired guanines and adenines are denoted by residue number and connected by dashed lines. The sheared m–M pair common to all examples is denoted by the double-dashed line. See Figure S2 for further details of the secondary structural diagrams.

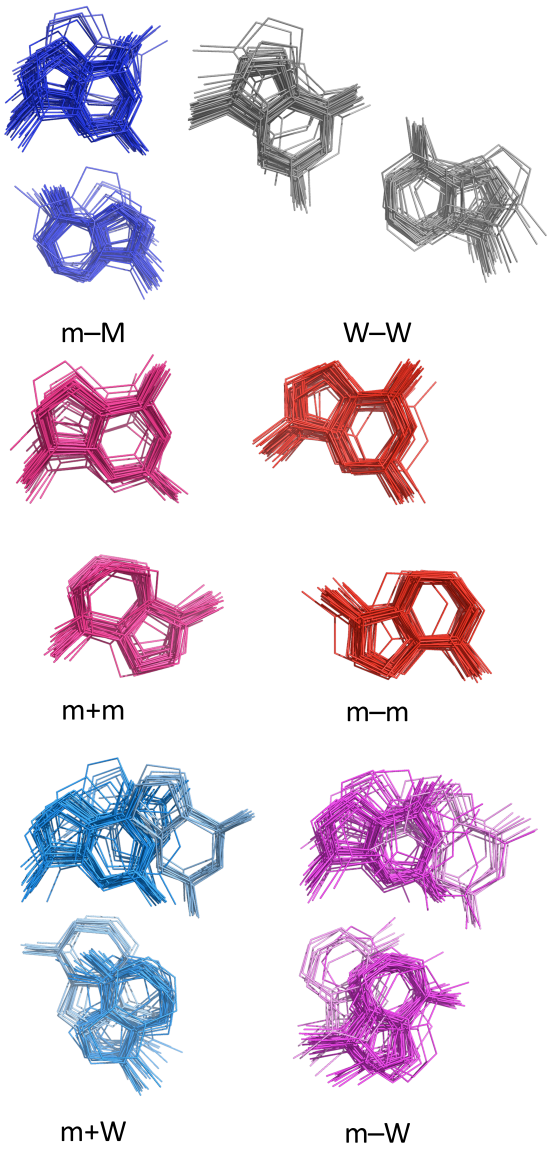

Figure S9. Visual comparison of the relative deformability of the bases comprised in the major G·A pairing schemes. The superimposed stick images are generated with 3DNA[11] using the observed rigid-body parameters of 50 representative examples and expressing the atomic coordinates in the middle frame of each base pair. Composite images are arranged in a top-down view perpendicular to the mean *xy* planes. Base pairs are color-coded as in Figures 1, 2 with minor (II) substates of m±W and m–M pairs denoted by lighter hues.

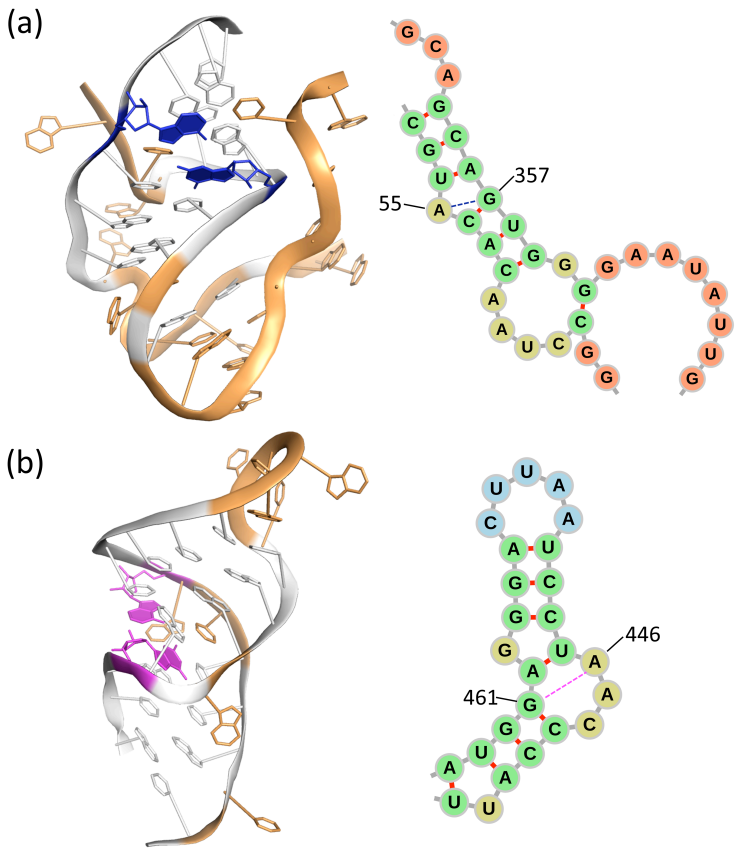

Figure S10.Molecular images (left) and simple secondary structural diagrams (right) illustrating overall changes in RNA spatial organization that accompany small changes in G·A base-pair association. (a) Single flipped-out adenine forming a sheared m–M_I pair with the guanine on the opposing side of a one-nucleotide bulge in the complex of tetracycline with the U1052G-muted 70S *Escherichia coli* ribosome;[12] (b) adenine at the 3´-terminus of a three-nucleotide bulge associated via m–W_{II} pairing with a similarly opposed guanine in the 80S *Saccharomyces cerevisiae* ribosome.[8] See Table S3 for respective Protein Data Bank identifiers and chain names of the depicted pairs and Figure S2 for further details of the secondary structural diagrams. G·A color-coding matches that in Figures 1, 2.

REFERENCES

(1) Berman, H. M., Westbrook, J., Feng, Z., Gilliland, G., Bhat, T. N., Weissig, H., Shindyalov, I. N., and Bourne, P. E. (2000) The Protein Data Bank, *Nucleic Acids Res. 28*, 235-242.

(2) Berman, H. M., Olson, W. K., Beveridge, D. L., Westbrook, J., Gelbin, A., Demeny, T., Hsieh, S.-H., Srinivasan, A. R., and Schneider, B. (1992) The Nucleic Acid Database: a comprehensive relational database of three-dimensional structures of nucleic acids, *Biophys. J. 63*, 751-759.

(3) Dickerson, R. E., Bansal, M., Calladine, C. R., Diekmann, S., Hunter, W. N., Kennard, O., von Kitzing, E., Lavery, R., Nelson, H. C. M., Olson, W. K., Saenger, W., Shakked, Z., Sklenar, H., Soumpasis, D. M., Tung, C.-S., Wang, A. H.-J., and Zhurkin, V. B. (1989) Definitions and nomenclature of nucleic acid structure parameters, *Nucleic Acids Res 17*, 1797-1803.

(4) Olson, W. K., Bansal, M., Burley, S. K., Dickerson, R. E., Gerstein, M., Harvey, S. C., Heinemann, U., Lu, X.-J., Neidle, S., Shakked, Z., Sklenar, H., Suzuki, M., Tung, C.-S., Westhof, E., Wolberger, C., and Berman, H. M. (2001) A standard reference frame for the description of nucleic acid base-pair geometry, *J Mol Biol 313*, 229-237.

(5) Lu, X.-J., Bussemaker, H. J., and Olson, W. K. (2015) DSSR: an integrated software tool for dissecting the spatial structure of RNA, *Nucleic Acids Res 43*, e142.

(6) Kerpedjiev, P., Hammer, S., and Hofacker, I. L. (2015) Forna (force-directed RNA): simple and effective online RNA secondary structure diagrams, *Bioinformatics 31*, 3377-3379.

(7) Polikanov, Y. S., Melnikov, S. V., Söll, D., and Steitz, T. A. (2015) Structural insights into the role of rRNA modifications in protein synthesis and ribosome assembly, *Nat Struct Mol Biol 22*, 342-344.

(8) Ben-Shem, A., Loubresse, N. G. d., Melnikov, S., Jenner, L., Yusupova, G., and Yusupov, M. (2011) The structure of the eukaryotic ribosome at 3.0 Å resolution, *Science 334*, 1524-1529.

(9) Serganov, A., Huang, L., and Patel, D. J. (2009) Coenzyme recognition and gene regulation by a flavin mononucleotide riboswitch, *Nature 458*, 233–237.

(10) Jaeger, L., Verzemnieks, E. J., and Geary, C. (2009) The UA_handle: a versatile submotif in stable RNA architectures, *Nucleic Acids Res 37*, 215-230.

(11) Lu, X.-J., and Olson, W. K. (2003) 3DNA: a software package for the analysis, rebuilding, and visualization of three-dimensional nucleic acid structures, *Nucleic Acids Res 31*, 5108-5121.

(12) Cocozaki, A. I., Altman, R. B., Huang, J., Buurman, E. T., Kazmirski, S. L., Doig, P., Prince, D. B., Blanchard, S. C., Cate, J. H. D., and Ferguson, A. D. (2016) Resistance mutations generate divergent antibiotic susceptibility profiles against translation inhibitors, *Proc Natl Acad Sci, USA 113*, 8188-8193.